Lipid mediated plant immunity in susceptible and tolerant soybean cultivars in response to *Phytophthora sojae* colonization and infection

Oludoyin Adeseun Adigun[1*], Thu Huong Pham[1], Dmitry Grapov[2], Muhammad Nadeem[1], Linda Elizabeth Jewell[3], Lakshman Galagedara[1], Mumtaz Cheema[1] and Raymond Thomas[4*]

Abstract

Background   Soybean is one of the most cultivated crops globally and a staple food for much of the world's population. The annual global crop losses due to infection by *Phytophthora sojae* is currently estimated at $20B USD, yet we have limited understanding of the role of lipid mediators in the adaptative strategies used by the host plant to limit infection. Since root is the initial site of this infection, we examined the infection process in soybean root infected with *Phytophthora sojae* using scanning electron microscopy to observe the changes in root morphology and a multi-modal lipidomics approach to investigate how soybean cultivars remodel their lipid mediators to successfully limit infection by *Phytophthora sojae*.

Results   The results reveal the presence of elevated biogenic crystals and more severe damaged cells in the root morphology of the infected susceptible cultivar compared to the infected tolerant cultivars. Furthermore, induced accumulation of stigmasterol was observed in the susceptible cultivar whereas, induced accumulation of phospholipids and glycerolipids occurred in tolerant cultivar.

Conclusion   The altered lipidome reported in this study suggest diacylglycerol and phosphatidic acid mediated lipid signalling impacting phytosterol anabolism appears to be a strategy used by tolerant soybean cultivars to successfully limit infection and colonization by *Phytophthora sojae*.

Keywords   *Glycine max* (soybean), Membrane lipids, Glycerolipids, Lipid mediators, Plant-pathogen interaction, *Phytophthora sojae*, Root and stem rot, Lipid network analysis

*Correspondence:
Oludoyin Adeseun Adigun
oaadigun@mun.ca
Raymond Thomas
rthomas2@uwo.ca
[1] School of Science and the Environment/Boreal Ecosystems and Agricultural Sciences, Grenfell Campus, Memorial University of Newfoundland, Corner Brook NL A2H 5G4, Canada
[2] CDS-Creative Data Solutions, Colfax, CA, USA
[3] St. John's Research and Development Centre, Agriculture and Agri-Food Canada, 204 Brookfield Road, St. John's, Newfoundland and Labrador A1E 6J5, Canada
[4] Department of Biology/Biotron Climate Change Experimental Research Centre, Western University, London, ON, Canada

Background

The global population is anticipated to increase to almost 9.7 billion by 2050, which will require a 70% increase in food production [1]. Food insecurity remains prevalent in many nations despite efforts to improve the production, the quality, and the availability of global food supplies [2]. Food insecurity is a major challenge that must be addressed to meet the demands of an ever-increasing global population [3]. To fulfill global food and feed requirements, innovative agricultural practices must be developed to enhance food production, availability and accessibility, which in turn will require advanced knowledge in plant pathology from seedling to crop harvest [4]. For instance, plant diseases are caused by infectious pathogens such as fungi, viruses, bacteria, and nematodes [4]. These diseases lead to significant annual economic losses in maize, potato, wheat, rice, and soybean worldwide accounting for a 40% yield reduction [4, 5]. Globally, approximately $20B USD are lost annually due to soybean root and stem rot disease caused by the oomycete *Phytophthora sojae* [6–9]. Soybean root and stem rot are the most devastating threat to seedling and plant survival affecting productivity, particularly during wet growing seasons [6, 8]. During the susceptible crop growth stages, pathogens can alter an otherwise favourable environment for the plant into unfavourable conditions, leading to significant yield losses [10]. The repeated applications and heavy dependence on synthetic chemicals such as fungicides limit effective long-term control of this disease, as well as pose serious environmental and human health risks [11]. Reducing the frequency and volume of chemical applications in agricultural crops is one of the primary objectives of plant pathological research. Hence, there is a need to develop innovative disease control systems improving the plant's natural defense mechanisms to build enduring and wide-spectrum disease resistance in crops to improve sustainable agriculture and food security [12, 13].

Plants respond to different biotic and abiotic stress conditions through various defense mechanisms that may be either constitutive or induced [4, 14]. The constitutive system utilizes pre-formed inhibitory chemicals such as alkaloids, saponins, and glycosides, and barriers like wax cuticles, cellulose and suberin to reduce pathogen entry [4, 8, 15]. Induced defense mechanisms are triggered by pathogen ingress causing plants to synthesize compounds or enzymes as a result of pathogen detection. This may occur at the site of infection by processes like the oxidative burst or the hypersensitive response, or the production of chitinases, nitric oxide or phytoalexins [4]. The plant cell wall is known to play multiple physiological roles during plant-pathogen interactions. The cell wall structurally consists of non-polysaccharides such as wax, lignin and carbohydrate-based polymers such as hemicellulose, cellulose in form of biogenic crystals, pectin, and chitin [8, 16]. Both hemicellulose and pectin are mixtures of highly branched polysaccharides in the cell wall of plants that spatially interact with each other [17]. The cellulose crystalline are bounded by hemicellulose and lignin [17]. These crystalline are crosslinked into a tough network of fibrous molecules that are responsible for mechanical and structural strength of the cell walls and play active role during plant response to environmental stimuli [18, 19]. Biogenic and biological crystals such as calcium oxalate are biosynthesized in various plant tissues, particularly during physiological and pathological processes [20, 21]. These crystals serve as support, protection, or defense in plants [20, 21]. In addition, plant cell walls contain different glycoproteins that are integrated into the matrix that are likely to provide more structural support to cell walls [22]. Plant glycoproteins are also involved in some biological functions during plant development and plant innate immunity. Furthermore, the response can be systemic in nature, producing pathogenesis-related proteins or the induction of systemic acquired resistance [23, 24]. Plants can also adapt to environmental stresses by regulating biochemical, physiological, and molecular properties of their cellular membrane [4, 25]. Several studies have demonstrated the roles of lipids in plant pathology as part of a complex internal defense mechanism in the fight against infections caused by various pathogens [4, 26–29]. Lipid remodeling is a defence mechanism adopted by plants to counteract pathogen attack [30]. Depending on the composition, lipid molecular species can regulate membrane fluidity, permeability, stability, and integrity during a plant's response to pathogenic microorganisms. For instance, free fatty acids (FA) such as linoleic acid and oleic acid, play active roles during biosynthesis of the plant cuticular wax, forming the first barrier against pathogens [27]. Lipid metabolites can also function as intracellular and extracellular signal mediators [27, 30]. Plant lipids include glycerophospholipids (GPL), phytosterols (PST), sphingolipids (SGL), glycoglycerolipids (GGL) and glycerolipids (GL) [4, 31–33], and their metabolites are actively involved in plant defence responses against pathogen colonization [34, 35]. They play important roles in the formation of the membrane interface between plant and the microbial pathogen [34, 35].

The GPLs of plant membranes possess two FAs as hydrophobic tails at the *sn1* and *sn2* carbons and a hydrophilic head group esterified to a phosphate group at the *sn3* position of the glycerol moiety. The classes of GPLs include phosphatidic acid (PA), phosphatidylcholine (PC), phosphatidylethanolamine (PE), phosphatidylglycerol (PG), phosphatidylinositol (PI),

and phosphatidylserine (PS). During plant-pathogen interactions, phospholipid-derived molecules rapidly accumulate and participate in plant signaling and membrane trafficking; they can also activate plant immunity [36, 37]. For instance, PA acts as a novel secondary messenger in plants and its biosynthesis has been reported to be triggered in response to pathogen attack [39, 40].

Plant sphingolipids are structural components of eukaryotic cellular membranes and play essential roles in maintaining membrane integrity [41]. They have been recently demonstrated to act as signaling molecules playing crucial functions in the regulation of pathophysiological processes [42–44]. Studies have demonstrated that sphingolipids play important roles during biotic stress in plants by activating defences against bacterial and fungal pathogens. For instance, the fungus *Alternaria alternata f. sp. lycopersici* has been shown to activate cell death through disruption of sphingolipid metabolism [45].

Phytosterols are integral components of cellular membranes and the most abundant sterols in plants include campesterol, sitosterol and stigmasterol [46]. Phytosterols are actively involved in regulation of membrane fluidity and integrity, and they influence membrane structural properties and physiological functions of plants. For instance, stigmasterol and beta-sitosterol play a vital role during structural formation and mediate cell membrane functions [47]. They have also been demonstrated to play essential roles in plant innate immunity against pathogen attack [48].

Galactolipids, including mono-/di-galactosyldiacylglycerol (MGDG and DGDG) are important membrane components in the chloroplasts of eukaryotic plants [49]. They play active roles in cell communication, signal transduction, and response to pathogen invasion [35].

Glycerolipids are actively required during cell growth and cell division [50], serve as energy storage for survival, participate in stress responses, and play an important role in reducing pathogenicity [51]. During environmental stresses in plants, triacylglycerol (TG) levels increase as a function of the sequestration of toxic lipid intermediates [52]. Studies have suggested that diacylglycerols (DGs) serve as signaling molecules during plant growth and development, and in response to stimuli during certain environmental stresses [53, 54]. In addition, DG and DG kinase are known to activate immunity during plant defence responses to pathogen attack [39]. Although the literature is replete with examples of the plant lipidome mediating plant defence, very little is known concerning how plant lipid mediators contributes to either successful colonization or tolerance in the soybean-*P. sojae* pathosystem.

In addition, lipids serve as structural components of cellular membranes, as well as provide carbon storage or energy, induce cell signaling pathways, and regulate stress responses during pathogenic infection [55, 56]. Lipid metabolism and lipid homeostasis are known to have systemic effects capable of influencing plant growth, survival and development during plant-pathogen interaction [57]. Several studies have documented plant–microbe interactions and the key changes characteristics of different pathosystems applying various "omics" techniques [29, 33, 58]. However, many questions regarding the communication and biochemical exchange between the plant and microbes during compatible and incompatible interactions is still unclear. Nonetheless, it is well known that pathogenic plant microbial recognition occurs at the cellular membrane. The cell membrane acts as the interface either allowing advantageous resource exchange or inhibiting interaction, as well as cell–cell communication through downstream signaling cascades [59, 60] mediated by anabolic or catabolic lipid metabolic reactions. Furthermore, the cell wall is the outermost boundary of the plant cell that either act as a preform or induced barrier to limit colonization upon microbe recognition and penetration [61] as the first line of defense. The cell membrane acts as a major biosensor critical in the perception and signaling responses to initial microbe recognition and downstream responses. The lipids in the cell membrane can be remodeled on the order of seconds to milliseconds or hours as part of the cascade of reactions mounted by the host plant to limit infection and colonization [62]. Concomitant with the altered membrane lipid metabolism, there are physical barriers on the plant cell surfaces that are either reinforced or induced to further limit the interaction between the host and microbe. These physical structures include calcium deposits, biogenic crystals, reinforced cell walls etc. that can also act as signaling molecules or sources of elicitors for recognition, thereby activating defense response against microbial colonization [29, 63, 64]". How these cell morphological changes converge as part of a lipid mediated plant immune response is a matter of great interest in many plant pathogen interactions or pathosystem, including the *soybean -P. sojae* pathosystem. We hypothesized that the morphological properties of the tolerant cultivar would suggest a mechanism for disease tolerance when compared to the morphological response in the susceptible cultivar and that the lipid mediated plant immunity in a *P. sojae*-tolerant soybean cultivar would fluctuate more than those of a *P. sojae*-susceptible cultivar following pathogen infection. To this end, we assessed the histochemical properties and lipidome of soybean root and stem to understand the functions
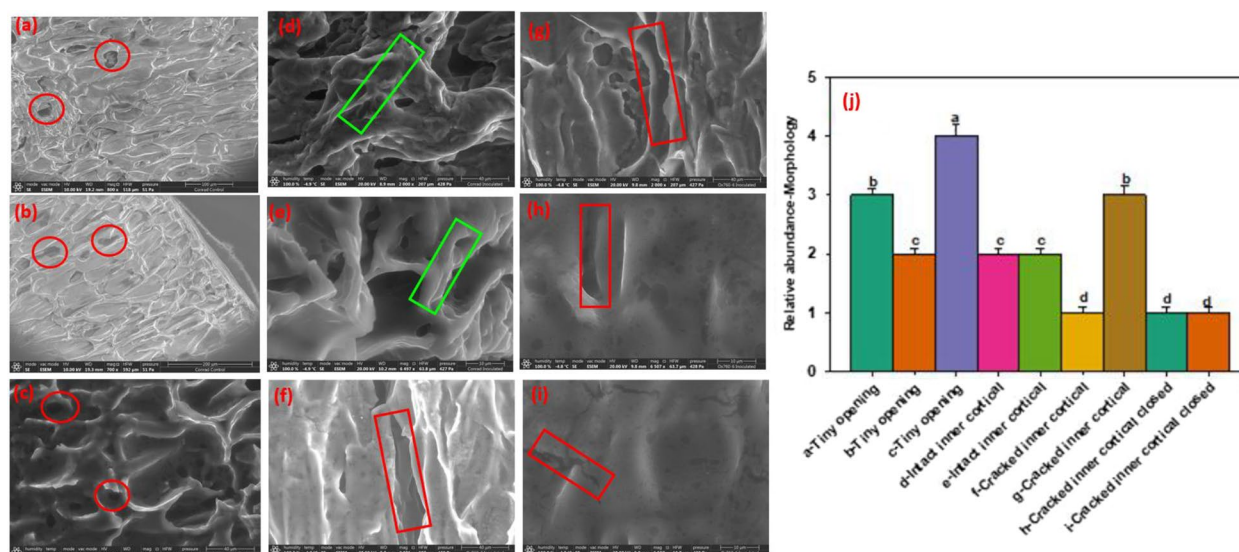
Fig. 1 Scanning electron microscopy (SEM) demonstrating morphology of soybean root segments. Tiny opening in the cortical cells indicated by red circle (**a-c**; 40–200 μm), intact inner cortical side of epidermis and cortex (**d**, **e**; 10, 40 μm), degradation and crack in the inner cortical side of epidermis and cortex (**f**, **g**; 40 μm), closing-up of degradation and crack in the inner cortical side of epidermis and cortex (**h**, **i**; 10 μm). Bar charts indicating the relative abundance of soybean root segments as mean ± SE (**j**; n > 5). Significant differences between morphology of soybean root segments are indicated using letters a-d on top of the bars following means separation using Fisher's LSD and ANOVA to assess significance of the model (α = 0.05)

of lipid mediators in the response of susceptible and tolerant soybean cultivars to pathogen colonization and infection.

Results

Histological changes in the root of both soybean cultivars infected with Phytophthora sojae.

To understand the morphological structure of soybean root and how changes occur in the morphology of the root during interaction with pathogens governing tolerance, scanning electron microscopy (SEM) was used to provide detailed images of soybean root morphology. Scanning electron microscopic images demonstrated opening in the cortex of the roots (Fig. 1a-c), the intact epidermis and cortical cell (Fig. 1d, e), degradation and crack in the cortical cells during interaction between soybean and *P. sojae* (Fig. 1f, g), and closing-up of degradation, crack in the inner cortical side of epidermis and cortex (Fig. 1h, i) and the relative abundance of soybean root segments (Fig. 1j). The tiny openings in the cortical cells were revealed in the non-infected and infected of both susceptible and tolerant soybean cultivars. Meanwhile, there were more opening in the infected susceptible cultivar than in the infected tolerant cultivar (Fig. 2a-d) similar changes in relative abundance of the tiny openings were also present in the cortical cells of the soybean root (Fig. 2a and e).

The SEM also revealed alterations of xylem walls. The cell walls of vascular cylinder of the susceptible cultivar were observed to be degraded after infection compared to the tolerant cultivar (Fig. 3a-d). It was seen that the vascular cylinder of tolerant cultivar was made up of thick cell walls demonstrating a physical response to confine or halt the pathogens from spreading further into the vascular cylinder compared to that of susceptible cultivar following infection with *P. sojae* (Fig. 3b, d) and the relative abundance of cells with thickened cell walls in the vascular cylinder of soybean root (Fig. 3e).

The SEM micrographs show biogenic crystals of different morphologies in various locations in the soybean roots of both susceptible and tolerant cultivars. Biogenic crystals of various morphologies are present in the xylem in copious amounts in the non-infected and infected susceptible cultivar and these crystals varied greatly in sizes (Fig. 4a, b). However, the amounts of the biogenic crystals observed in non-infected susceptible root remained unchanged in the infected susceptible root. (Fig. 4a, b). In contrast, the crystals were observed to be present in copious amounts in the root of non-infected tolerant cultivar relative to the root of infected tolerant cultivar (Fig. 4c, d). Therefore, it was observed that biogenic crystals found in the roots of the infected susceptible cultivar were present in more copious amounts than in the infected tolerant cultivar (Fig. 4b, d) and vise-visa to their non-infected
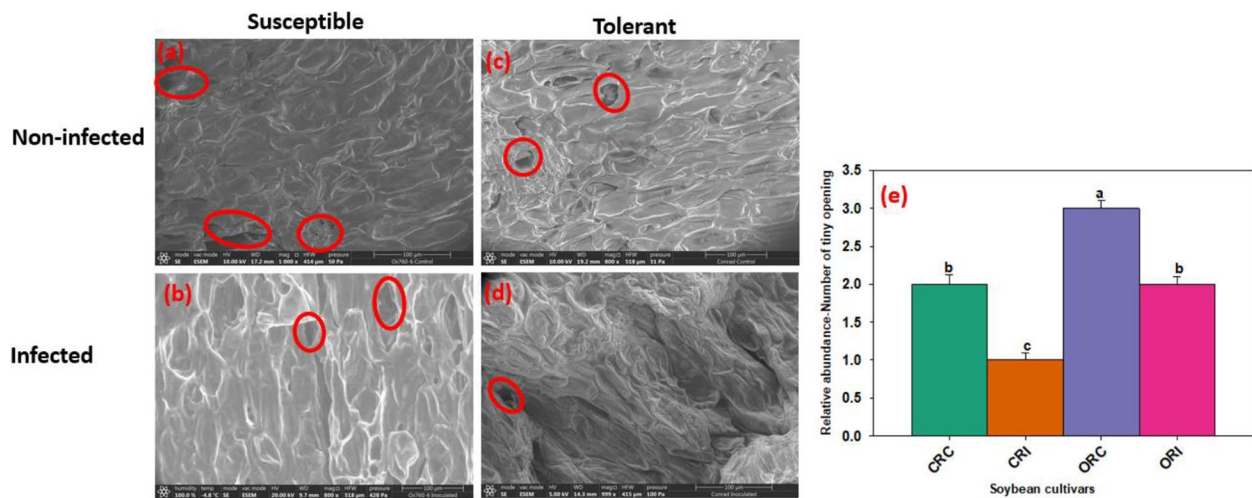
Fig. 2 Scanning electron microscopy showing the tiny opening of root cortical cells of susceptible and tolerant soybean cultivars when inoculated with *P. sojae*. Tiny opening of cortical cells of the non-infected susceptible soybean cultivar (ORC; **a**), infected susceptible soybean cultivar (ORI; **b**), non-infected tolerant soybean cultivar (CRC; **c**), infected tolerant soybean cultivar (CRI; **d**). Red circles denote the tiny opening of epidermal cells of the roots. The tiny opening of epidermal cells appears to be larger in the susceptible cultivar compared to tolerant cultivar after infection. Bars: (**a**-**d**) 100 µm. Bar charts indicating the relative abundance of the tiny openings present in the cortical cells of soybean root as mean ± SE (e; n > 5). Significant differences between the treatments are indicated using letters (a-d) on top of the bars following means separation using Fisher's LSD and ANOVA to assess significance of the model (α = 0.05)
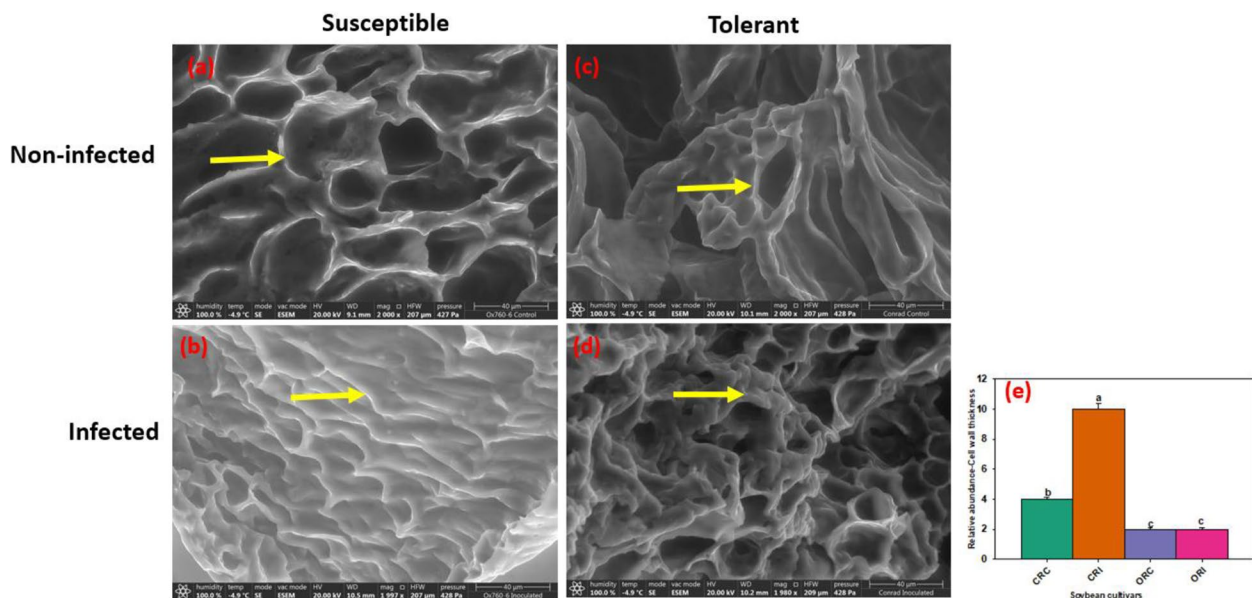
Fig. 3 Scanning electron microscopy showing the cell walls of vascular cylinder of the susceptible and the tolerant soybean cultivars when inoculated with *P. sojae*. **a** Cell wall of vascular cylinder of the non-infected susceptible soybean cultivar, (**b**) Cell wall of vascular cylinder of the infected susceptible soybean cultivar, (**c**) Cell wall of vascular cylinder of the non-infected tolerant soybean cultivar, (**d**) Cell wall of vascular cylinder of the infected tolerant soybean cultivar. The cell wall of vascular cylinder of the infected tolerant cultivar observed to be thicker compared to the cell wall of vascular cylinder of the susceptible cultivar. Bars: (a-d) 40 µm. Bar charts indicating the relative abundance of cells with thickened cell walls in the vascular cylinder of soybean root as mean ± SE (e; n > 5). Significant differences between the treatments are indicated using letters (**a**-**d**) on top of the bars as described by Fisher's LSD and ANOVA (α = 0.05)

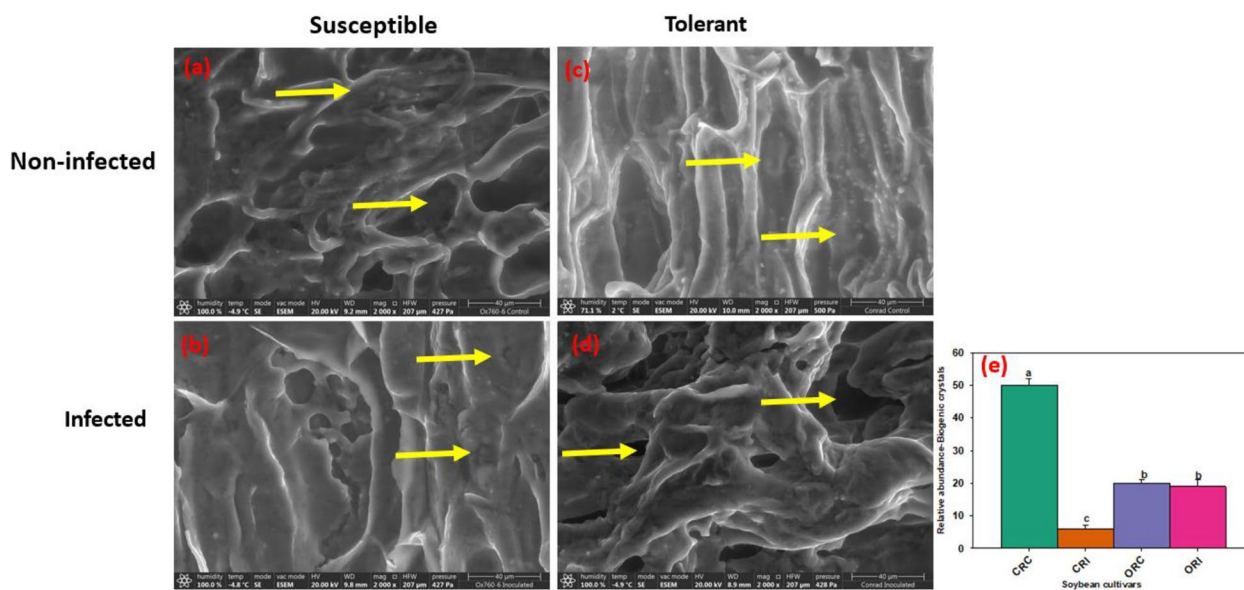Adigun *et al. BMC Plant Biology*   (2024) 24:154

Page 6 of 26

Fig. 4 Scanning electron microscopy showing the presence of biogenic crystals in the root tissues of susceptible and tolerant soybean cultivars when inoculated with *P. sojae*.**a** Cross section of the non-infected susceptible soybean cultivar, (**b**) Cross section of the infected susceptible soybean cultivar, (**c**) Cross section of the non-infected tolerant soybean cultivar, (**d**) Cross section of the infected tolerant soybean cultivar. Yellow arrows denote the presence of biogenic crystals in the vascular cylinder in copious amounts in both non-infected susceptible and tolerant cultivars. Biogenic crystals were present in the vascular cylinder in copious amounts in the non-infected and infected susceptible cultivar, and in non-infected tolerant cultivar but their quantity was reduced in infected tolerant cultivar. Bars: (**a-d**) 40 μm. Bar charts indicating the relative abundance of biogenic crystals in the vascular cylinder of soybean root as mean ± SE (**e**; n > 5). Significant differences between treatments showing biogenic crystals in the vascular cylinder of soybean root are indicated using letters (**a-d**) on top of the bars as described by Fisher's LSD and ANOVA (α = 0.05)

counterparts (Fig. 4a, c), the relative abundance of biogenic crystals in the vascular cylinder of soybean root (Fig. 4e).

Lipid composition of the soybean cultivars in response to P. sojae infection

We applied a multi-modal lipidomics approach using UHPLC-C30RP-HESI-HRAM-MS/MS to obtain a detailed understanding of how susceptible and tolerant soybean cultivars remodeled their lipid mediators to successfully limit infection by *P. sojae* using 10-day old seedlings as a model. The results confirmed as hypothesized that there are significant alterations in the root and stem lipidomes within and between susceptible and tolerant soybean cultivars following inoculation with pathogenic *P. sojae* (Tables 1, 2). Representative chromatograms and mass spectrum demonstrating the separation of the membrane and storage lipids present in the root and stem of the soybean cultivars evaluated (negative and positive ion modes) is shown in Fig. 5. The chromatograms of separated membrane lipids in negative ion mode are shown in Fig. 5a. The extracted ion chromatogram of *m/z* 671.46, 802.56 and 833.52 precursor ions of the three selected polar lipids are shown in Fig. 5b. The MS^2 spectrum of *m/z* 671.46 identified as PA 16:0/18:2 [M-H]$^-$ is depicted in Fig. 5c.

For example, m/z 152 represent the glycerol moiety (head group) in PA and m/z 255 and 279 represent C16:0 and C18:2 fatty acids present in PA 16:0/18:2 (Fig. 5c). The same convention was used in identifying the other lipids present in Fig. 5. This included *m/z* 802.56 identified as PC 16:0/18:2 [M + HCOO]$^-$ in Fig. 4d, m*/z* 833.52 representing PI 16:0/18:2 [M-H]$^-$ in Fig. 5e. Together, these accounted for some of the main membrane lipids identified in the soybean plant tissue. Similarly, a chromatogram demonstrating the separation of GLs from the stem of the soybean cultivar in the positive ion mode is shown in Fig. 5f. The extracted ion chromatogram of m/z 630.51, 890.72 and 892.74 representing the precursor ions of the three selected GLs are depicted in Fig. 5g. The MS^2 spectrum of *m/z* 630.51 identified as DG 18:3/18:3 [M + NH$_4$]$^+$ is depicted in Fig. 5h, the MS^2 spectrum of *m/z* 802.56 identified as TG 18:3/18:3/18:3 [M + NH$_4$]$^+$ is depicted in Fig. 5i, and the MS^2 spectrum of *m/z* 833.52 representing TG 18:3/18:2/18:3 [M + NH$_4$]$^+$ is depicted in Fig. 5j. These species account for some of the major GLs identified in the plant tissue. Further diagnostic chromatograms demonstrating the characteristic product ions of some biomarkers differentiating the root and stem lipidomes of the soybean cultivars, identified

Adigun *et al. BMC Plant Biology*   (2024) 24:154

Page 7 of 26

Table 1 Effect of *Phytophthora sojae* infection on the root lipidome of susceptible and tolerant soybean cultivars

Lipid classes	Lipid sub-classes	Relative abundance (nmole%)			
		ORC	ORI	CRC	CRI
Glycerophospholipids	PC*	25.67 ± 0.84^c	24.47 ± 1.78^d	29.87 ± 1.10^b	31.12 ± 0.20^a
	PE*	25.77 ± 0.25^a	24.66 ± 2.47^b	20.46 ± 2.39^d	23.07 ± 0.52^c
	PA*	5.50 ± 0.51^d	6.75 ± 0.95^c	9.17 ± 1.38^b	12.91 ± 0.69^a
	PG^{ns}	3.90 ± 0.98	3.62 ± 0.49	3.80 ± 0.54	3.76 ± 0.60
	PI*	7.94 ± 0.49^a	7.09 ± 0.59^a	1.51 ± 0.45^c	3.52 ± 0.33^b
	PS*	1.32 ± 0.30^a	1.26 ± 0.30^a	0.27 ± 0.12^b	1.44 ± 0.20^a
	LPC^{ns}	0.15 ± 0.01	0.18 ± 0.02	0.25 ± 0.03	0.36 ± 0.04
	LPE^{ns}	0.03 ± 0.00	0.04 ± 0.01	0.04 ± 0.01	0.04 ± 0.00
Glycerolipids	TG*	19.03 ± 0.55^b	19.10 ± 0.03^b	28.16 ± 3.48^a	14.05 ± 1.02^c
	DG*	6.90 ± 0.16^c	8.40 ± 0.50^a	4.73 ± 0.18^d	7.74 ± 0.30^b
Phytosterols	AcHexSiE*	1.06 ± 0.34^a	0.77 ± 0.26^b	0.07 ± 0.03^c	0.04 ± 0.00^c
	SiE^{ns}	0.55 ± 0.09	0.47 ± 0.04	0.07 ± 0.04	0.03 ± 0.02
	AcHexStE^{ns}	0.05 ± 0.10	0.04 ± 0.02	0.05 ± 0.01	0.03 ± 0.01
	AcHexCmE^{ns}	0.09 ± 0.04	0.04 ± 0.02	ND	ND
	CmE^{ns}	0.04 ± 0.01	0.03 ± 0.01	0.01 ± 0.00	ND
	StE*	0.13 ± 0.01^c	1.08 ± 0.02^a	0.46 ± 0.07^b	0.12 ± 0.10^c
Sphingolipids	HexCer*	1.12 ± 0.08^a	1.35 ± 0.16^a	0.51 ± 0.42^b	1.37 ± 0.25^a
	Cer^{ns}	0.31 ± 0.02	0.29 ± 0.04	0.47 ± 0.03	0.30 ± 0.05
	SM^{ns}	0.01 ± 0.00	0.01 ± 0.00	0.07 ± 0.10	0.08 ± 0.02
Glycoglycerolipid	MGDG^{ns}	0.44 ± 0.14	0.35 ± 0.20	0.03 ± 0.01	0.02 ± 0.01
Total		**100.00**	**100.00**	**100.00**	**100.00**
Glycerophospholipids*		$\mathbf{70.28 \pm 0.28^b}$	$\mathbf{68.07 \pm 0.96^c}$	$\mathbf{65.37 \pm 0.27^b}$	$\mathbf{76.22 \pm 0.25^a}$
Glycerolipids*		$\mathbf{25.93 \pm 0.20^c}$	$\mathbf{27.50 \pm 0.55^b}$	$\mathbf{32.89 \pm 2.17^a}$	$\mathbf{21.79 \pm 1.03^d}$
Phytosterols*		$\mathbf{1.91 \pm 0.02^b}$	$\mathbf{2.43 \pm 0.02^a}$	$\mathbf{0.66 \pm 0.02^c}$	$\mathbf{0.22 \pm 0.09^d}$
Sphingolipids*		$\mathbf{1.44 \pm 0.04^a}$	$\mathbf{1.65 \pm 0.18^a}$	$\mathbf{1.05 \pm 0.02^b}$	$\mathbf{1.75 \pm 0.20^a}$
Glycoglycerolipid^{ns}		$\mathbf{0.44 \pm 0.14}$	$\mathbf{0.35 \pm 0.20}$	$\mathbf{0.03 \pm 0.01}$	$\mathbf{0.02 \pm 0.01}$

Values in the table (nanomole% by weight composition) denote means ± standard errors for four biological replicates. Means in the same row with different superscripts are indicated as significantly different (*significant at alpha = 0.05) or not significantly different (ns) between the treatments, which consisted of susceptible control (OSC) and inoculated (OSI) stem tissue; and tolerant control (CSC) and inoculated (CSI) stem tissue from 10-day old seedlings, at a significance level of α < 0.05. The lipids detected were: *PA* Phosphatidic acid, *PE* Phosphatidyl- ethanolamine, *PC* Choline, *PG* Glycerol, *PS* Serine, *PI* Inositol, *TG* Triacylglycerol, *DG* Diacylglycerol, *LPC* Lysophosphatidylcholine, *LPE* Lysophosphatidylethanolamine, *SM* Sphingomyelin, *MGDG* Monogalactosyldiacylglycerol, *SiE* Beta sitosterol, *StE* Stigmasterol ester, *HexCer* Hexosyl ceramide, *Cer* Ceramide, *CmE* Campesterol ester, *AcHexStE* Acylated hexosyl stigmasterol ester, *AcHexSiE* Acylated hexosyl betasitosterol ester, and *AcHexCmE* Acylated hexosyl campesterol ester. Lipids that were not detected (ND) under the treatment conditions are indicated

from their lipid biochemical network (Table S2, Figs S4, S5, S6, S7 and S8).

We observed five lipid classes: GPL, PST, GL, SGL, and GGL in soybean stem and root. Glycerophospholipids accounted for the highest portion of total lipids in both cultivars, irrespective of tissue type or inoculation status, representing 65.37 ± 0.27 nmol% to 76.22 ± 0.25 nmol% of all lipids in root (Table 1) and 66.56 ± 1.32 to 80.67 ± 2.15 nmol% in stem (Table 2), followed by GLs which ranged from 21.79 ± 1.03 nmol% to 32.89 ± 2.17 nmol% in the roots and 16.11 ± 1.13 nmol% to 24.90 ± 1.51 nmol% in the stems (Table 2). Phytosterols, SGLs, and GGLs were present in lower quantities ranging between 0.02 ± 0.01 nmol% to 2.43 ± 0.02 nmol% for root (Table 1) and 0.47 ± 0.07 nmol% to 4.18 ± 0.66 nmol% for

stem (Table 2). From the five lipid classes investigated, 20 subclasses were analyzed across both root and stem which include eight GPLs, two GLs, six PSTs, three SGLs, and one GGL (Tables 1, 2). In tolerant root tissue, the percentage of the following lipids increased after inoculation: PC (4.18%), PE (12.76%), PA (40.79%), PI (133.11%), PS (433.33%), hexaceramide (HexCer; 168.63%), and DG (63.64%) (Table 1). In contrast, the following lipid increases were observed in the susceptible roots: PA (22.73%), DG (21.74%) and stigmasterol ester (StE; 730.77%) (Table 1). In the stem of the tolerant cultivar, an increase in lipid levels was observed for PC (13.16%), PE (5.05%), PA (59.36%), PI (8.85%), HexCer (67.00%), and DG (69.85%) whereas in susceptible cultivar's stem, an increase in lipid levels was observed

Adigun *et al. BMC Plant Biology* (2024) 24:154

Page 8 of 26

Table 2 Effect of *Phytophthora sojae* infection on stem lipidome of susceptible and tolerant soybean cultivars

Lipid classes	Lipid sub-classes	Relative abundance (nmole%)			
		OSC	OSI	CSC	CSI
Glycerophospholipids	PC*	22.05 ± 2.50^{b}	17.52 ± 0.92^{c}	20.98 ± 0.26^{b}	23.74 ± 0.39^{a}
	PE*	33.89 ± 2.13^{a}	27.45 ± 1.48^{b}	21.18 ± 0.18^{d}	22.25 ± 0.61^{c}
	PA*	2.72 ± 1.27^{d}	7.60 ± 1.52^{c}	8.39 ± 0.20^{b}	13.37 ± 1.88^{a}
	PG*	8.77 ± 1.16^{c}	7.80 ± 0.41^{d}	12.30 ± 0.69^{a}	10.72 ± 1.56^{b}
	PI*	5.16 ± 0.59^{c}	4.54 ± 0.50^{d}	6.67 ± 0.41^{b}	7.26 ± 0.64^{a}
	PS*	2.24 ± 0.66^{b}	1.25 ± 0.63^{c}	5.33 ± 0.76^{a}	2.91 ± 0.40^{b}
	LPC[ns]	0.42 ± 0.04	0.32 ± 0.03	0.38 ± 0.04	0.36 ± 0.05
	LPE[ns]	0.09 ± 0.00	0.08 ± 0.02	0.09 ± 0.00	0.06 ± 0.01
Glycerolipids	TG*	10.11 ± 1.25^{d}	16.55 ± 0.02^{b}	17.89 ± 1.50^{a}	11.66 ± 2.00^{c}
	DG*	7.78 ± 1.15^{b}	8.35 ± 0.72^{a}	2.62 ± 0.10^{d}	4.45 ± 0.12^{c}
Phytosterols	AcHexSiE[ns]	0.55 ± 0.06	0.72 ± 0.14	0.11 ± 0.02	0.60 ± 0.01
	SiE*	1.14 ± 0.25^{a}	0.46 ± 0.20^{b}	0.68 ± 0.11^{a}	0.41 ± 0.05^{b}
	AcHexStE[ns]	0.75 ± 0.37	0.69 ± 0.21	0.04 ± 0.00	0.05 ± 0.01
	AcHexCmE[ns]	0.14 ± 0.05	0.20 ± 0.03	0.01 ± 0.00	ND
	CmE[ns]	0.44 ± 0.12	0.15 ± 0.05	0.01 ± 0.00	0.01 ± 0.01
	StE*	0.34 ± 0.16^{b}	1.98 ± 0.02^{a}	0.33 ± 0.05^{b}	0.40 ± 0.15^{b}
Sphingolipids	HexCer*	0.89 ± 0.17^{b}	1.96 ± 0.02^{a}	1.00 ± 0.08^{b}	1.67 ± 0.03^{a}
	Cer[ns]	0.27 ± 0.06	0.31 ± 0.02	0.71 ± 0.04	0.21 ± 0.03
	SM[ns]	ND	ND	0.03 ± 0.01	0.01 ± 0.00
Glyceroglycolipid	MGDG*	2.25 ± 0.08^{a}	2.09 ± 0.06^{a}	1.25 ± 0.18^{b}	0.47 ± 0.07^{c}
Total		**100.00**	**100.00**	**100.00**	**100.00**
Glycerophospholipids*		$\mathbf{75.34 \pm 1.20^{b}}$	$\mathbf{66.56 \pm 1.32^{c}}$	$\mathbf{75.32 \pm 1.22^{b}}$	$\mathbf{80.67 \pm 2.15^{a}}$
Glycerolipids*		$\mathbf{17.89 \pm 0.25^{c}}$	$\mathbf{24.90 \pm 1.51^{a}}$	$\mathbf{20.51 \pm 1.60^{b}}$	$\mathbf{16.11 \pm 1.13^{d}}$
Phytosterols*		$\mathbf{3.36 \pm 0.12^{b}}$	$\mathbf{4.18 \pm 0.66^{a}}$	$\mathbf{1.18 \pm 0.19^{c}}$	$\mathbf{0.86 \pm 0.06^{d}}$
Sphingolipids*		$\mathbf{1.16 \pm 0.03^{c}}$	$\mathbf{2.27 \pm 0.05^{a}}$	$\mathbf{1.74 \pm 0.12^{b}}$	$\mathbf{1.89 \pm 0.06^{b}}$
Glyceroglycolipid*		$\mathbf{2.25 \pm 0.08^{a}}$	$\mathbf{2.09 \pm 0.06^{a}}$	$\mathbf{1.25 \pm 0.18^{b}}$	$\mathbf{0.47 \pm 0.07^{c}}$

Values in the table (nanomole% by weight composition) denote means ± standard errors for four biological replicates. Means in the same row with different superscripts are indicated as significantly different (*significant at alpha = 0.05) or not significantly different (ns) between the treatments, which consisted of susceptible control (OSC) and inoculated (OSI) stem tissue; and tolerant control (CSC) and inoculated (CSI) stem tissue from 10-day old seedlings, at a significance level of $\alpha < 0.05$. The lipids detected were: *PA* Phosphatidic acid, *PE* Phosphatidyl- ethanolamine, *PC* Choline, *PG* Glycerol, *PS* Serine, *PI* inositol, *TG* triacylglycerol, *DG* Diacylglycerol, *LPC* Lysophosphatidylcholine, *LPE* Lysophosphatidylethanolamine, *SM* Sphingomyelin, *MGDG* Monogalactosyldiacylglycerol, *SiE* Beta sitosterol, *StE* Stigmasterol ester, *HexCer* Hexosyl ceramide, *Cer* Ceramide, *CmE* Campesterol ester, *AcHexStE* Acylated hexosyl stigmasterol ester, *AcHexSiE* Acylated hexosyl betasitosterol ester, and *AcHexCmE* Acylated hexosyl campesterol ester. Lipids that were not detected (ND) under the treatment conditions are indicated

for PA (179.41%), DG (7.33%), TG (63.70%), HexCer (120.22%) and StE (482.35%) (Table 2). Specifically, we observed significantly higher levels of major GPLs, HexCer and DG in the tolerant cultivar, but higher levels of TG and StE in the susceptible cultivar in response to *P. sojae* colonization and infection.

Modification of membrane lipids in soybean cultivars in response to P. sojae infection

An analysis of membrane lipids in soybean root and stem tissues following infection with *P. sojae* was performed to determine changes and modification of membrane lipids during host–pathogen interaction. Figures 6a-d and 7a-d demonstrate the changes that occurred in membrane lipids during host–pathogen interactions. Based upon the membrane lipid molecular species observed, we conducted PLS-DA to determine the most important membrane lipid molecular species with influential loadings (Figs. 6a, b and 7a, b) segregating the tolerant from the susceptible cultivar based on pathogen challenge. The model quality (Q^2) represents 95% and 96% variability in root and stem, respectively (Fig. 6a, 7a). The result from the PLS-DA observation plot showed the segregation of the susceptible and tolerant soybean cultivars before and after infection into four distinct groups that are in accordance with the root and stem membrane lipid molecular species (Fig. 6b, 7b). The root membrane lipid molecular species (Fig. 6b) separated the treatments into four distinct quadrants (Q). Quadrant
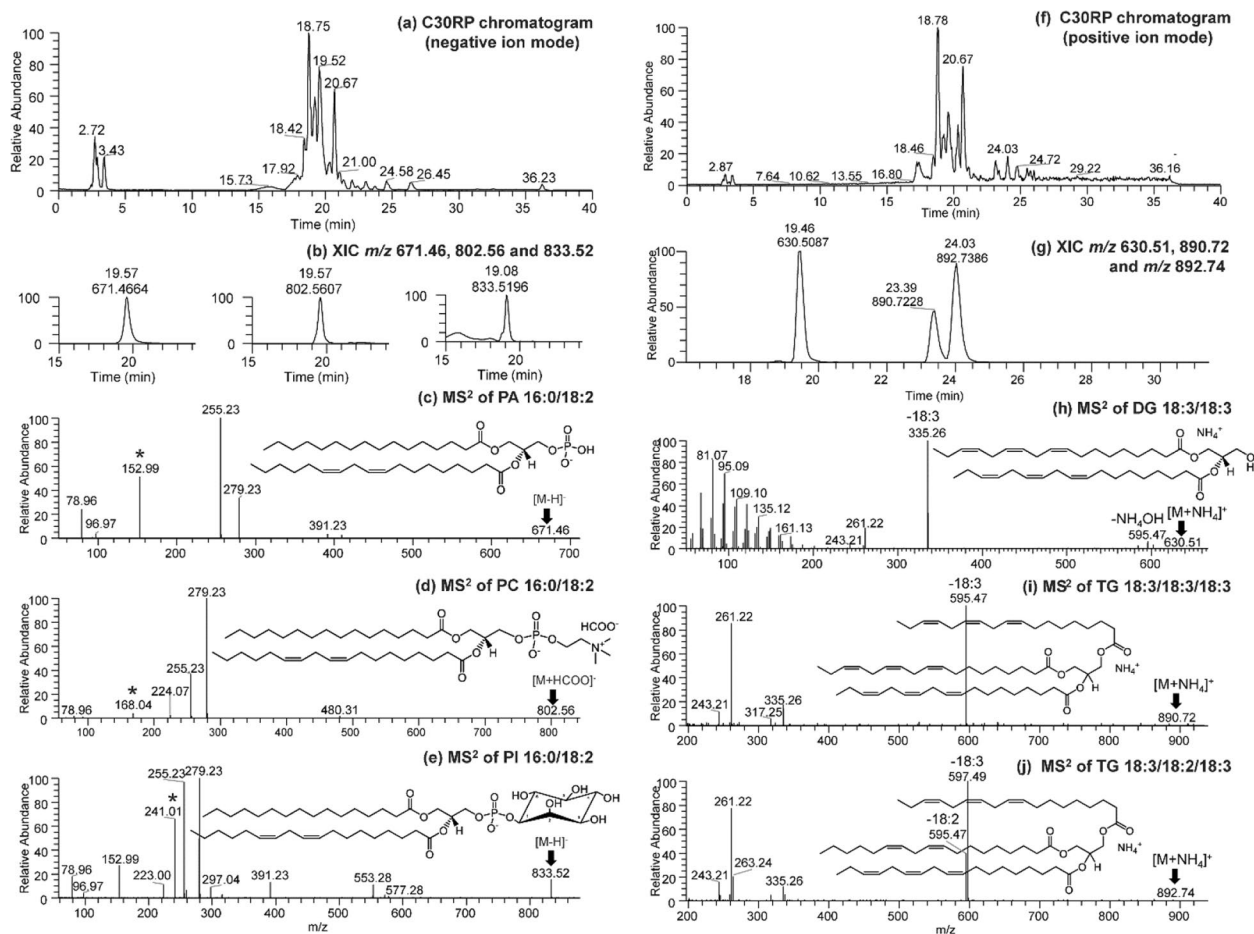
Adigun *et al. BMC Plant Biology* (2024) 24:154

Page 9 of 26

Fig. 5 Chromatogram demonstrating the UHPLC-C30RP-HESI-HRAM-MS separation of the membrane lipids and glycerolipids in the root and stem of susceptible and tolerant soybean cultivars. **a** LC–MS chromatogram of separated membrane lipids in negative ion mode, (**b**) Extracted ion chromatogram (XIC) of *m/z* 671.46, 802.56 and 833.52 precursor ions of the three selected polar lipids, (**c**) MS^2 spectrum of *m/z* 671.46 identified as PA 16:0/18:2 [M-H]$^-$, (**d**) MS^2 spectrum of *m/z* 802.56 identified as PC 16:0/18:2 [M+HCOO]$^-$ and (**e**) MS^2 spectrum of *m/z* 833.52 representing PI 16:0/18:2 [M-H]$^-$ identified in the negative ion mode; (**f**) LC–MS chromatogram in positive ion mode of separated glycerolipids in positive ion mode (**g**) Extracted ion chromatogram (XIC) of *m/z* 630.51, 890.72 and 892.74 precursor ions of the three selected glycerolipids, (**h**) MS^2 spectrum of *m/z* 630.51 identified as DG 18:3/18:3 [M+NH$_4$]$^+$, (**i**) MS^2 spectrum of *m/z* 802.56 identified as TG 18:3/18:3/18:3 [M+NH$_4$]$^+$ and (**j**) MS^2 spectrum of *m/z* 833.52 representing TG 18:3/18:2/18:3 [M+NH$_4$]$^+$ identified in the positive ion mode. PA=phosphatidic acid, PC=phosphatidylcholine, and PI=phosphatidylinositol, DG=diacylglycerol, TG=triacylglycerol, and * represent the head group for each of the lipid class presented

1 contained the lipid molecular species associated with Conrad root control (CRC) treatment, Q-2 contained Conrad root inoculated (CRI) treatment, Q-3 contained OX760-6 root control (ORC) and Q-4 had the OX760-6 root inoculated (ORI) treatment, respectively. Similarly, the changes in soybean stem (Fig. 6b), lipid molecular species separated the treatments into 4 distinct quadrants (Q-1, Q-2, Q-3 and Q-4) consisting of Conrad stem control (CSC), Conrad stem inoculated (CSI), OX760-6 stem control (OSC) and OX760-6 stem inoculated (OSI) treatments, respectively.

Based upon Component 3, which demonstrated the highest variation in the data (Figs. 6a, 7a), 22 membrane

lipid molecular species from root tissue and 21 membrane lipid molecular species from stem tissue were selected for further analysis. Heat maps (Figs. 6c, 7c) were generated for the lipids with influential loadings accounting for the genotype and treatment segregation to further classify the treatments based on the altered membrane lipidome following infection. The cut-off value for variables important in projection (VIP) scores was defined as > 1 [32, 65]. The 22 important root membrane lipid molecular species and 21 important stem membrane lipid molecular species were selected based on VIP scores greater than 1. The output from the heat map analysis showed four different clusters of the soybean root
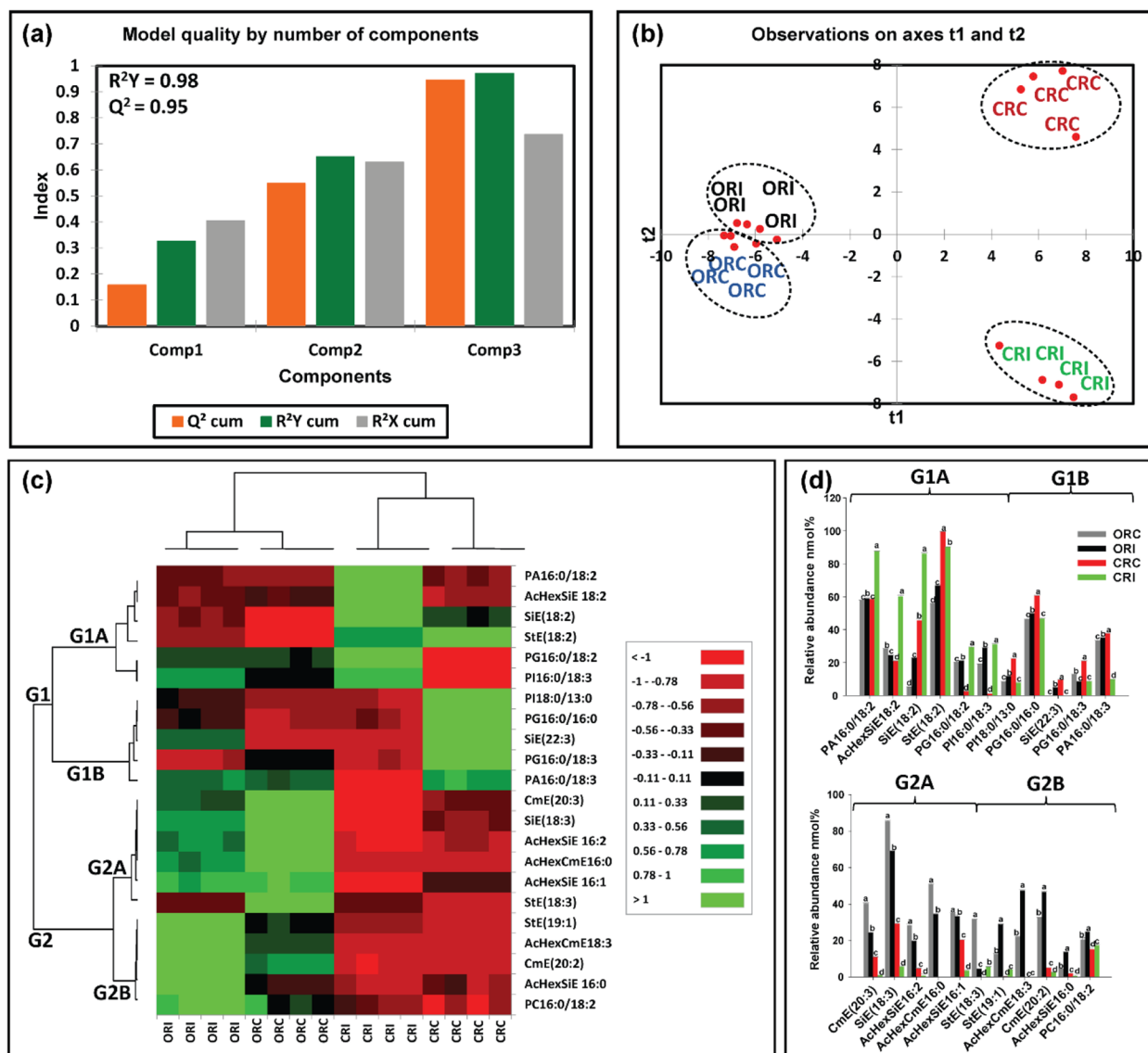
Fig. 6 Differences in root membrane lipids in susceptible (OX760-6) and tolerant (Conrad) soybean cultivars inoculated with *P. sojae* relative to control plants. **a** Model quality for partial least squares-discriminant analysis (PLS-DA); (**b**) Observation plot based upon differences in molecular species in root membrane lipids of OX760-6 and Conrad cultivars; (**c**) Heat map demonstrating clusters of root membrane lipid species in OX760-6 and Conrad cultivars treated or untreated with *P. sojae*. Each cultivar and treatment were grouped separately using ascendant hierarchical cluster analysis based upon Euclidian distance at interquartile range of 0.15. The left columns denote the cluster segregated root membrane lipid species, while the above columns segregated soybean cultivars based upon similarities in abundance. The abundance of root membrane lipid species is denoted using color: red for lower level, black for intermediate level, and green for higher level. Group 1 and 2 (G1 and G2) and subgroups (G1A, G1B, G2A and G2B) are root membrane lipid species that were accountable for the formation of clustered patterns in the heat map that were applied for determination of significant differences between the soybean cultivars (OX760-6 and Conrad) root membrane lipid species in each of the bar chart (Fig. 5d) beside the heat map; and (**d**) Bar charts describe the relative abundance of root membrane lipid species as a mean nmol% ± SE (*n* = 4). Significant differences between root membrane lipid species are indicate using letter a-d on top of the bars as described by Fisher's LSD multiple comparisons test using ANOVA (α = 0.05). The G1 and G2, and G1A, G1B, G2A and G2B are root membrane lipid species that were accountable for the formation of clustered patterns in the heat map that were applied for the determination of significant differences between the soybean cultivars (OX760-6 and Conrad) root membrane lipid species as illustrated in the bar charts. The susceptible cultivar, ORC (non-infected) & ORI (infected), and the tolerant cultivar CRC (non-infected) & CRI (infected)
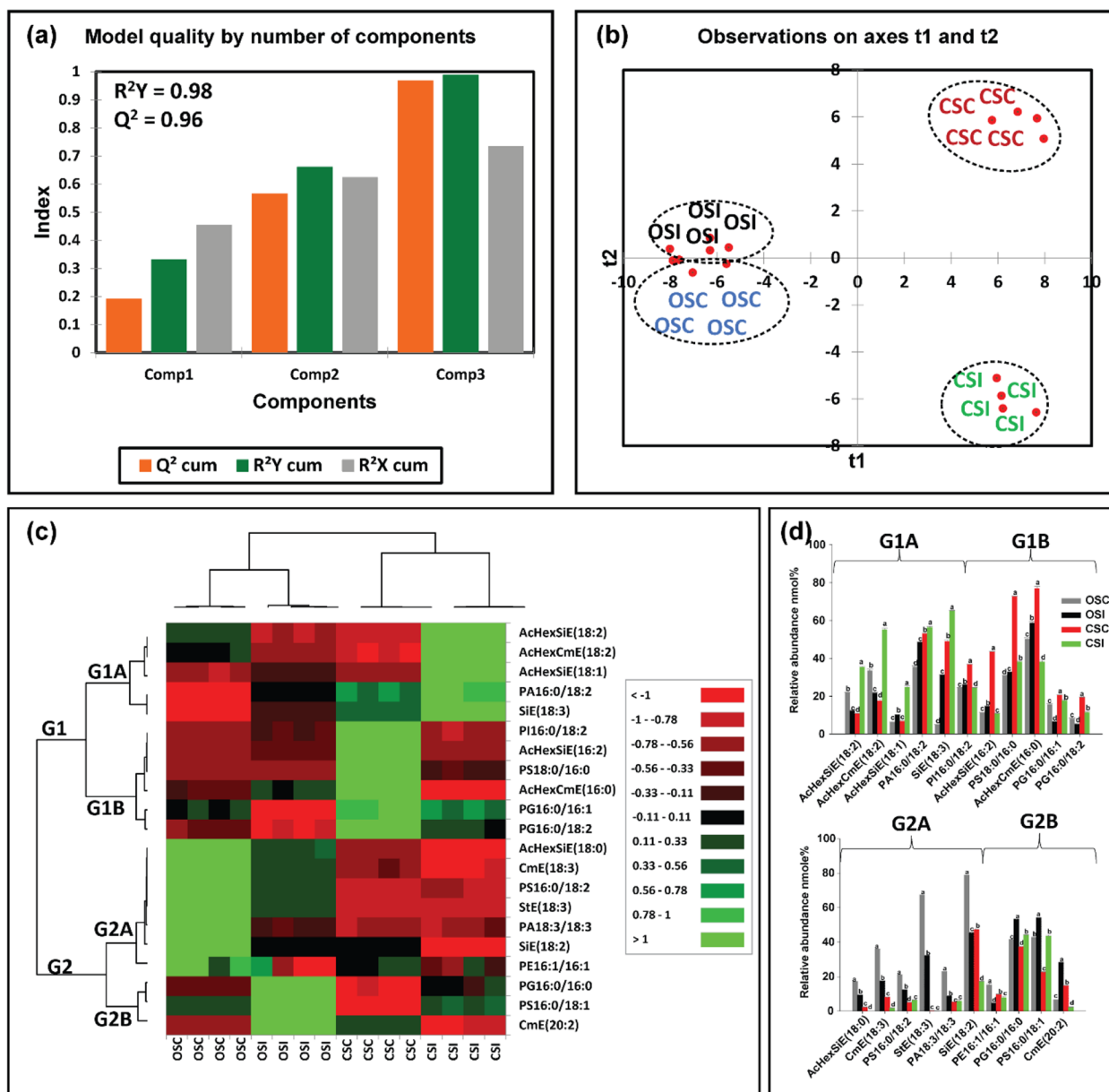
Fig. 7 Differences in stem membrane lipids in susceptible (OX760-6) and tolerant (Conrad) soybean cultivars inoculated with *P. sojae* relative to control plants. **a** Model quality for partial least squares-discriminant analysis (PLS-DA); (**b**) Observation plot based upon differences in molecular species in stem membrane lipids of OX760-6 and Conrad cultivars; (**c**) Heat map demonstrating clusters of stem membrane lipid species in OX760-6 and Conrad cultivars treated or untreated with *P. sojae*. Each cultivar and treatment were grouped separately using ascendant hierarchical cluster analysis based upon Euclidian distance at interquartile range of 0.15. The left columns denote the cluster segregated stem membrane lipid species, while the above columns segregated soybean cultivars based upon similarities in abundance. The abundance of stem membrane lipid species is denoted using color: red for lower level, black for intermediate level, and green for higher level. Group 1 and 2 (G1 and G2) and subgroups (G1A, G1B, G2A and G2B) are stem membrane lipid species that were accountable for the formation of clustered patterns in the heat map that were applied for determination of significant differences between the soybean cultivars (OX760-6 and Conrad) stem membrane lipid species in each of the bar chart (Fig. 4d) beside the heat map; and (**d**) Bar charts describe the relative abundance of stem membrane lipid species as a mean nmol%±SE (n=4). Significant differences between stem membrane lipid species are indicate using letter a-d on top of the bars as described by Fisher's LSD multiple comparisons test using ANOVA (α=0.05). The G1 and G2, and G1A, G1B, G2A and G2B are stem membrane lipid species that were accountable for the formation of clustered patterns in the heat map that were applied for the determination of significant differences between the soybean cultivars (OX760-6 and Conrad) stem membrane lipid species as illustrated in the bar charts. The susceptible cultivar, ORC (non-infected) & ORI (infected), and the tolerant cultivar CRC (non-infected) & CRI (infected)

and stem membrane lipid molecular species following inoculation with *P. sojae* (Figs. 6c, 7c).

The heat map clusters root membrane lipid species into two main groups (G), G1 and G2, and four sub-groups, G1A, G1B, G2A and G2B. These groupings distinguished the susceptible cultivar (ORC & ORI) from the tolerant cultivar (CRC & CRI) in the root membrane lipid species in response to infection. We observed differences in the root membrane lipid species in G1A, where the relative abundance (nmol%) of PA(16:0/18:2), AcHex-SiE(18:2), SiE(18:2), PG(16:0/18:2), PI(16:0/18:3) were significantly elevated in the tolerant cultivar challenged with *P. sojae* relative to the control and the susceptible cultivar (Fig. 2c). Lipid molecular species belonging to group G1B {PI(18:0/13:0), PG(16:0/16:0), SiE(22:3), PG(16:0/18:3), and PA(16:0/18:3)} were significantly lower in the tolerant cultivar that was challenged with the pathogen, whereas there was no difference in the susceptible cultivar whether treated or untreated with the pathogen (Fig. 6c). Lipid molecular species belonging to group G2A {CmE(20:3), SiE(18:3), AcHexSiE(16:2), AcHexCmE(16:0), AcHexSiE(16:1) and StE(18:3)} were not different in the root of the tolerant cultivar when treated or untreated with the pathogen, but were significantly lower in the root of susceptible cultivar challenged with the pathogen (Fig. 6c). Finally, in G2B, the relative abundances of StE(19:1), AcHexCmE(18:3), CmE(20:2), AcHexSiE(16:0), and PC(16:0/18:2) were not significantly different in the root of the tolerant cultivar but were significantly higher in the root of the susceptible cultivar infected by the pathogen (Fig. 6c). These data are corroborated by Fig. 6d, which demonstrates the significant differences in the molecular species in the root of tolerant and susceptible cultivars. In the pathogen challenged roots of the tolerant cultivar, the relative abundances of PA(16:0/18:2), AcHexSiE(18:2), PG(16:0/18:2), PG(16:0/18:3), (StE18:3) and (PC(16:0/18:2) were higher, whereas the relative abundances of StE (18:2), SiE(22:3), StE (19:1), AcHexCmE(18:3), CmE(20:2), AcHex-SiE(16:0), and (PC(16:0/18:2) were lower in the root of susceptible cultivar infected with the pathogen (Fig. 6d).

Similarly, the heat map clusters stem membrane lipid molecular species into two major groups (G1and G2) which are further divided into sub-groups G1A, G1B, G2A and G2B. These groupings distinguished the susceptible cultivar (OSC & OSI) from the tolerant cultivar (CSC & CSI) in the stem membrane lipid molecular species. We observed stem membrane lipid molecular species in the tolerant cultivar, corresponding to G1A and consisting of AcHexSiE(18:2), AcHexCmE(18:2), AcHex-SiE(18:1), PA(16:0/18:2), and SiE(18:3), were significantly higher in the tolerant cultivar challenged with *P. sojae* but there were no significant differences in the lipids of the

susceptible cultivar. On the other hand, PA(16:0/18:2) was higher in the pathogen-infected tissue relative to the control (Fig. 7c). Lipid molecular species belonging to G1B {(PI(16:0/18:2), AcHexSiE(16:2), PS(18:0/16:0), AcHexCmE(16:0), PG(16:0/16:1), and PG(16:0/18:2)} were significantly lower in the tolerant cultivar challenged with the pathogen, whereas there was no difference in the susceptible cultivar regardless of infection status (Fig. 7c). Lipid molecular species belonging to G2A {AcHexSiE(18:0), CmE(18:3), PS(16:0/18:2), StE(18:3), PA(18:3/18:3), SiE(18:2) and PE(16:1/16:1)} were not significantly different in the stem of the tolerant cultivar but were significantly lower in the stem of susceptible cultivar challenged with the pathogen. Finally, in G2B, the levels of PG(16:0/16:0), PS(16:0/18:1) and CmE(20:2) significantly increased in the stem of the susceptible cultivar challenged with *P. sojae* (Fig. 7c). These trends are further corroborated by the output presented in Fig. 7d, which demonstrates the significant differences in the molecular species in the stem of tolerant and susceptible cultivar when challenged with the pathogen. For example, AcHexSiE(18:2), AcHexCmE(18:2), AcHexSiE(18:1), SiE(18:3), PS(16:0/18:2), and PA(18:3/18:3) were significantly higher in the stem of the tolerant cultivar, whereas AcHexSiE(18:1), AcHexSiE(16:2), AcHexCmE(16:0), and CmE(20:2) were significantly higher in the stem of the susceptible cultivar (Fig. 7d). These results showed there were significantly higher levels of GPL molecular species in root and stem of tolerant cultivar whereas there were significantly higher relative levels of PST molecular species in the root and stem of the susceptible cultivar in response to infection by the pathogen.

Modification of glycerolipids in soybean cultivars in response to P. sojae infection

We also analysed GL in soybean root and stem tissues following infection with *P. sojae* to determine whether their levels and composition were altered during host–pathogen interaction (Figs. 8a-d, 9a-d). Triacylglycerols and DGs were observed to be the major GLs present regardless of soybean cultivar. We next performed PLS-DA to identify the most important TG and DG species with influential loadings (Figs. 8a, b, 9a, b) segregating the tolerant and susceptible soybean cultivars in their response to *P. sojae* colonization and infection. The model quality (Q^2) represents 80% and 83% variability in root and stem, respectively (Fig. 8a, 9a). The result from the PLS-DA observation plot showed the segregation of the susceptible and tolerant soybean cultivars that were infected or not infected with the pathogen into four distinct quadrants based on the levels of GL molecular species (Figs. 8b, 9b). The root GL molecular species (Fig. 8b) separated the treatments into
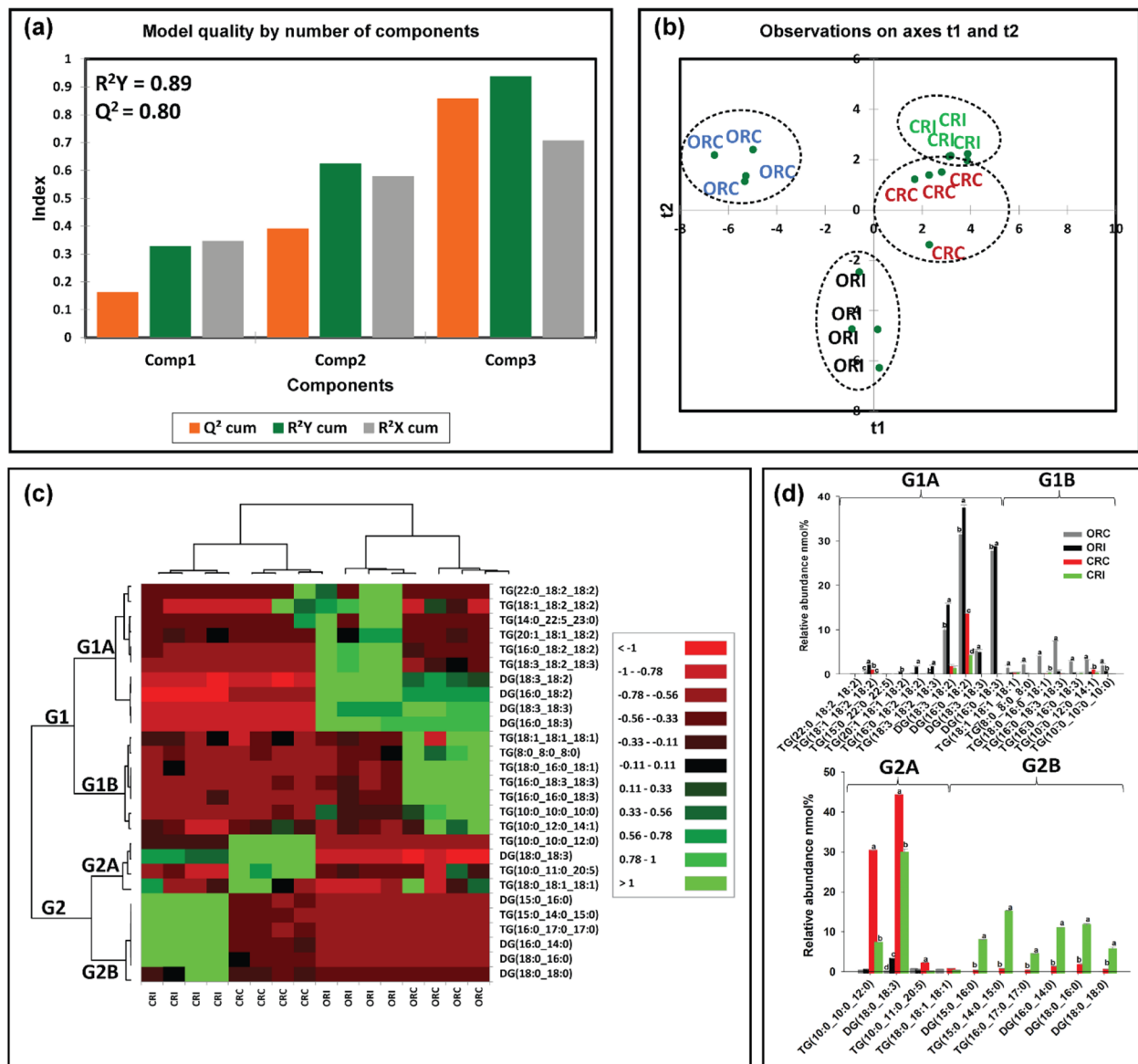
Fig. 8 Differences in root glycerolipid species in susceptible (OX760-6) and tolerant (Conrad) soybean cultivars inoculated with *P. sojae* relative to control plants. **a** Model quality for partial least squares-discriminant analysis (PLS-DA); (**b**) Observation plot based upon differences in molecular species in root glycerolipid species of OX760-6 and Conrad cultivars; (**c**) Heat map demonstrating clusters of root glycerolipid species in OX760-6 and Conrad cultivars treated or untreated with *P. sojae*. Each cultivar and treatment were grouped separately using ascendant hierarchical cluster analysis based upon Euclidian distance at interquartile range of 0.15. The left columns denote the cluster segregated root glycerolipid species, while the above columns segregated soybean cultivars based upon similarities in abundance. The abundance of root glycerolipid species is denoted using color: red for lower level, black for intermediate level, and green for higher level. Group 1 and 2 (G1 and G2) and subgroups (G1A, G1B, G2A and G2B) are root glycerolipid species that were accountable for the formation of clustered patterns in the heat map that were applied for determination of significant differences between the soybean cultivars (OX760-6 and Conrad) root glycerolipid species in each of the bar chart (Fig. 7d) beside the heat map; and (**d**) Bar charts describe the relative abundance of root glycerolipid species as a mean nmol%±SE (*n*=4). Significant differences between root glycerolipid species are indicate using letter a-d on top of the bars as described by Fisher's LSD multiple comparisons test using ANOVA (α=0.05). The G1 and G2, and G1A, G1B, G2A and G2B are root glycerolipid species that were accountable for the formation of clustered patterns in the heat map that were applied for the determination of significant differences between the soybean cultivars (OX760-6 and Conrad) root glycerolipid species as illustrated in the bar charts. The susceptible cultivar, ORC (non-infected) & ORI (infected), and the tolerant cultivar CRC (non-infected) & CRI (infected)
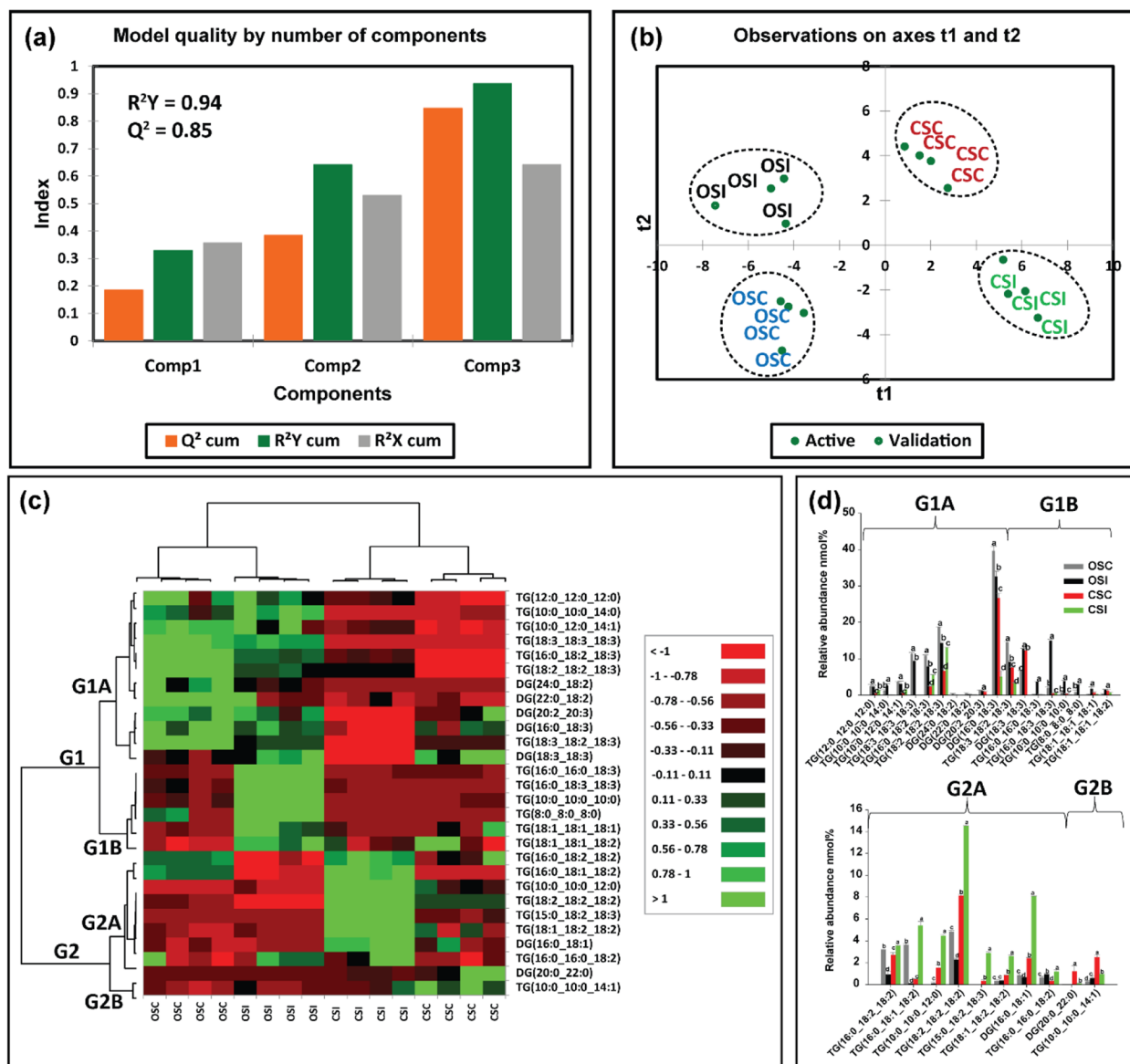
Fig. 9 Differences in stem glycerolipid species in susceptible (OX760-6) and tolerant (Conrad) soybean cultivars inoculated with *P. sojae* relative to control plants. **a** Model quality for partial least squares-discriminant analysis (PLS-DA); (**b**) Observation plot based upon differences in molecular species in stem glycerolipid species of OX760-6 and Conrad cultivars; (**c**) Heat map demonstrating clusters of stem glycerolipid species in OX760-6 and Conrad cultivars treated or untreated with *P. sojae*. Each cultivar and treatment were grouped separately using ascendant hierarchical cluster analysis based upon Euclidian distance at interquartile range of 0.15. The left columns denote the cluster segregated stem glycerolipid species, while the above columns segregated soybean cultivars based upon similarities in abundance. The abundance of stem glycerolipid species is denoted using color: red for lower level, black for intermediate level, and green for higher level. Group 1 and 2 (G1 and G2) and subgroups (G1A, G1B, G2A and G2B) are stem glycerolipid species that were accountable for the formation of clustered patterns in the heat map that were applied for determination of significant differences between the soybean cultivars (OX760-6 and Conrad) stem glycerolipid species in each of the bar chart (Fig. 8d) beside the heat map; and (**d**) Bar charts describe the relative abundance of stem glycerolipid species as a mean nmol%±SE (*n*=4). Significant differences between stem glycerolipid species are indicate using letter a-d on top of the bars as described by Fisher's LSD multiple comparisons test using ANOVA (α=0.05). The G1 and G2, and G1A, G1B, G2A and G2B are stem glycerolipid species that were accountable for the formation of clustered patterns in the heat map that were applied for the determination of significant differences between the soybean cultivars (OX760-6 and Conrad) stem glycerolipid species as illustrated in the bar charts. The susceptible cultivar, ORC (non-infected) & ORI (infected), and the tolerant cultivar CRC (non-infected) & CRI (infected)

Adigun *et al. BMC Plant Biology*   (2024) 24:154

Page 15 of 26

four distinct quadrants. Quadrants 1–4 were composed of the GL molecular species of CRC, CRI, ORC and ORI treatments, respectively. Similar to the changes in soybean stem (Fig. 9b), GL species separated the treatments into 4 distinct quadrants (Q1-Q4) consisting of the GLs from CSC, CSI, OSC and OSI, respectively.

Based upon component 3 which explained the highest level of variation in the data (Figs. 8a, 9a), 27 GL molecular species from root tissues and 28 GL molecular species from the stem tissue with VIPs greater than 1 were selected for further multivariate analysis. Heat maps (Figs. 8c, 9c) were next generated for the lipids with influential loadings accounting for the genotype and treatment segregation to further classify the treatments based on the altered GL in the infected tissue. The output from the heat map analysis showed four different clusters of the soybean root and stem membrane lipid molecular species following inoculation with *P. sojae* (Figs. 8c, 9c). The heat map clustered GL species into two main groups, G1 and G2, and four sub-groups (G1A, G1B, G2A and G2B). These groupings distinguished the GL lipid molecular species in the root of the susceptible cultivar (ORC and ORI) from those of the root of the tolerant cultivar (CRC and CRI), as well as the stem-derived GL lipid molecular species from both the susceptible (OSC and OSI) and tolerant cultivar (CSC and CSI) (Figs. 8, 9).

We observed that root GL molecular species in G1A {TG(22:0/18:2/18:2), TG(18:1/18:2/18:2), TG(18:3/18:2/23:0), TG(20:1/18:1/18:2), TG(16:0/18:2/18:2), TG(18:3/18:2/18:3), DG(18:3/18:2), DG(16:0/18:2), DG(18:3/18:3), and DG(16:0/18:3)} did not differ in the tolerant cultivar challenged with *P. sojae* relative to control, but were significantly higher in the susceptible cultivar challenged with the pathogen (Fig. 8c). Lipid molecular species belonging to group G1B {TG(18:1/18:1/18:1), TG(8:0/8:0/8:0), TG(18:0/16:0/18:1), TG(16:0/18:3/18:3), TG(16:0/16:0/18:3), TG(10:0/12:0/14:1), and TG(10:0/10:0/10:0)} also did not differ in the tolerant cultivar regardless of infection status, but were significantly lower in the susceptible cultivar in response to infection (Fig. 8c). In contrast, lipid molecular species belonging to group G2A {TG(10:0/10:0/12:0), DG(18:0/18:3), TG(18:4/11:3/12:4), and TG(18:0/18:1/18:1)} were significantly lower in the root of the tolerant cultivar that was challenged with the pathogen, but no differences were observed for the susceptible cultivar regardless of infection status (Fig. 8c). Finally, in G2B, the relative abundances of DG(15:0/16:0), TG(15:0/14:0/15:0), TG(16:0/17:0/17:0), DG(16:0/14:0), DG(18:0/16:0) and DG(18:0/18:0) were significantly higher in the tolerant cultivar in response to infection, whereas no differences were observed for the susceptible cultivar regardless of infection status(Fig. 8c). These data are corroborated by Fig. 8d, which demonstrates the significant differences in the molecular

species in the root of tolerant and susceptible cultivars. In response to pathogen challenge, TG(18:0/16:0/18:1), DG(15:0/16:0), TG(15:0/14:0/15:0), TG(16:0/17:0/17:0), DG(16:0/14:0), DG(18:0/16:0) and DG(18:0/18:0) were significantly higher in the root of the tolerant cultivar while TG(18:1/18:2/18:2), TG(20:1/18:1/18:2), TG(16:0/18:2/18:2), TG(18:3/18:2/18:3), DG(18:3/18:2), DG(16:0/18:2), DG(18:0/18:3) were significantly higher in the root of the susceptible cultivar after infection (Fig. 8d).

Likewise, the heat map clusters stem GL lipid molecular species into G1and G2, and sub-groups G1A, G1B, G2A and G2B. These groupings distinguished the susceptible cultivar from the tolerant cultivar in the stem GL molecular species. We observed stem GL lipid molecular species that belonged to G1A {TG(12:0/12:0/12:0), TG(10:0/10:0/14:0), TG(10:0/10:0/14:1), TG(18:3/18:3/18:3), TG(16:0/18:2/18:3), TG(18:2/18:2/18:3), DG(24:0/18:2), DG(22:0/18:2), DG(20:2/20:3), DG(16:0/18:3) TG(18:3/18:2/18:3), and DG(18:3/18:3)} did not change in the tolerant cultivar challenged with *P. sojae* relative to the control, but were significantly lower in the susceptible cultivar that had been infected (Fig. 9c). Lipid molecular species belonging to group G1B {TG(16:0/16:0/18:3), TG(16:0/18:3/18:3), TG(10:0/10:0/10:0), TG(8:0/8:0/8:0), TG(18:1/18:1/18:1), TG(18:1/18:1/18:2)} also did not differ among the tolerant cultivar, but were significantly higher in the susceptible cultivar that had been treated with the pathogen (Fig. 9c). In contrast, lipid molecular species belonging to group G2A {TG(16:0/18:2/18:2), TG(16:0/18:1/18:2), TG(10:0/10:0/12:0), TG(18:2/18:2/18:2), TG(15:0/18:2/18:3), TG(18:1/18:2/18:2), DG(16:0/18:1), and TG(16:0/16:0/18:2)} were significantly higher in the stem of the tolerant cultivar that had been challenged with the pathogen, but no significant differences were observed in the stem of susceptible cultivar (Fig. 9c). Finally, in G2B, the relative abundances of DG(20:0/22:0) and TG(10:0/10:0/14:1) were significantly lower in the stem of the tolerant cultivar when challenged with *P. sojae* but did not differ among the susceptible cultivar (Fig. 9c). These data are corroborated by Fig. 9d, which demonstrates the significant differences in the GL molecular species in the stem of tolerant and susceptible cultivars. In response to pathogen challenge, TG(12:0/12:0/12:0), TG(10:0/10:0/14:1), TG(16:0/18:2/18:3), TG(18:2/18:2/18:3), TG(16:0/18:2/18:2), TG(16:0/18:1/18:2), TG(10:0/10:0/12:0), TG(18:2/18:2/18:2), TG(15:0/18:2/18:3), TG(18:1/18:2/18:2), DG(16:0/18:1), and TG(16:0/16:0/18:2) were significantly higher in the stem of the tolerant cultivar while TG(10:0/10:0/14:0), DG(18:3/18:3), TG(16:0/16:0/18:3), TG(16:0/18:3/18:3), TG(18:3/18:2/18:3), TG(10:0/10:0/10:0), TG(8:0/8:0/8:0), TG(18:1/18:1/18:1), TG(18:1/18:1/18:2) and TG(16:0/16:0/18:2) were significantly higher in the stem of the susceptible cultivar in response to infection (Fig. 9d). These results showed that there were significantly higher levels of TG and DG molecular species in root and stem of tolerant cultivar challenged with the

pathogen compared to the stem of the susceptible cultivar following infection.

Lipid biochemical network demonstrating from a system biology perspective how the tolerant and susceptible soybean cultivars respond to P. sojae infection

Lipid structural similarity networks were used to visualize changes in soybean root and stem lipids. For instance, the networks display three major clusters including top left (PSTs), top right (DGs and TGs containing saturated FAs), and bottom (a mixture of GPLs, DGs and TGs containing unsaturated FAs. CME 20:3 is the precursor for the biosynthesis of all the PSTs in the pathway presented, the level was significantly decrease resulting in downstream decrease in all unsaturated acylated hexocyl sitosterols. StE 18:3 had the biggest decrease in the ORC vs. ORI network of PST. In contrast, StE 18:3 increased several folds in CRC vs. CRI network, and it had the biggest increase. Generally, almost all the PSTs were decreased in the tolerant cultivar in response to infection. In the ORC vs ORI network,

TG8:0/8:0/8:0, TG18:0/16:0/18:1, TG16:0/18:3/18:3, TG16:0/18:3/18:3 and TG16:0/16:0/18:3 are unique biomarkers differentiating the ORC vs. ORI while TG18:4/11:3/12:4 and DG18:0/18:0 were unique biomarkers differentiating CRC vs. CRI (Fig. 10). In OSC vs. OSI, StE 18:3 is a precursor for biosynthesis of all the PSTs, the level was significantly reduced leading upstream increase in all unsaturated acylated hexocyl sitosterols. AcHexSiE18:2 and AcHexSiE18:1 was increased several folds in CRC vs. CRI network. Similar to the root, almost all the PSTs in stem were reduced in the tolerant cultivar compared to the susceptible cultivar. In OSC vs. OSI, DG22:0/18:2 was the only unique biomarker differentiating OSC vs. OSI while in the CSC vs. CSI, TG12:0/12:0/12:0, TG16:0/16:0/18:2, TG10:0/10:0/14:1 and DG20:0/22:0 were unique biomarkers differentiating CSC vs. CSI (Fig. 11). In the ORI vs. CRI, TG10:0/10:0/10:0, TG(18:3/18:2/23:0), DG 18:3/18:3 and DG16:0/18:3 were unique biomarkers differentiating ORI vs. CRI and TG10:0/10:0/14:0 and DG24:0/18:2 were unique biomarkers differentiating OSI
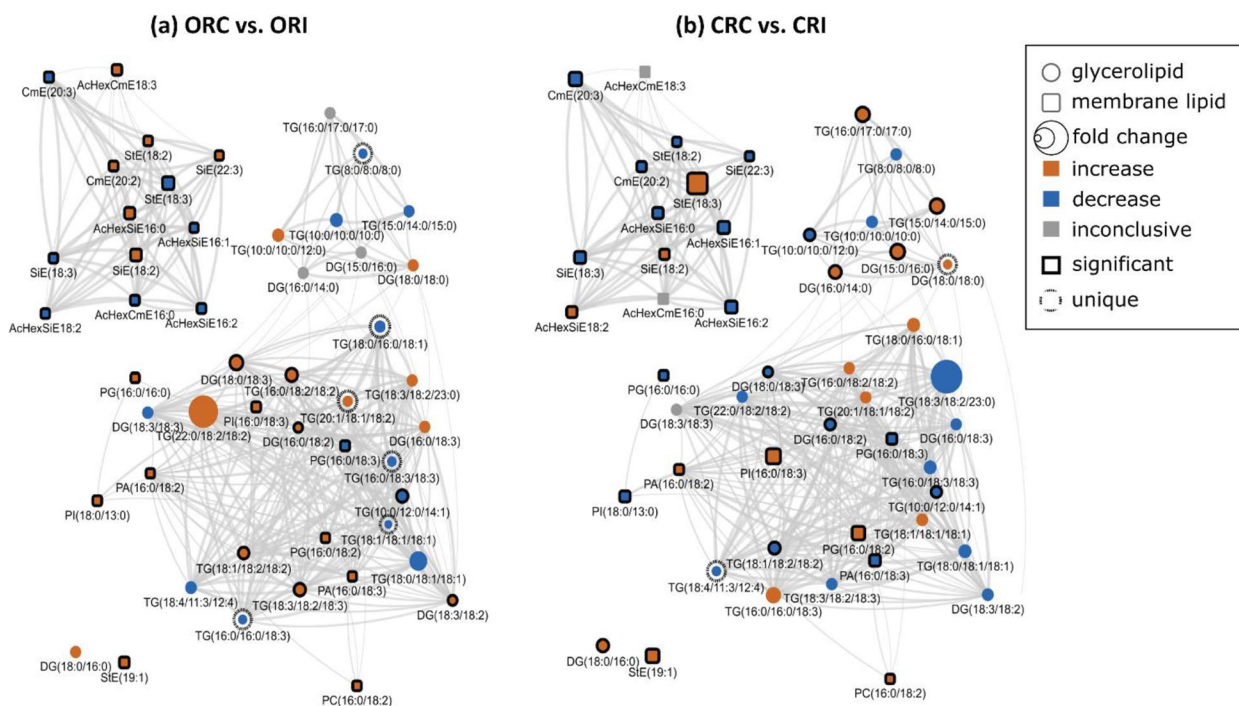

Fig. 10 Lipid biochemical network displaying differences in storage and membrane lipids in the root of susceptible and tolerant soybean cultivars inoculated with *P. sojae* relative to control plants. **a** Control susceptible soybean cultivar (ORC) versus inoculated (ORI); **b** control tolerant soybean cultivar (CRC) versus inoculated (CRI). The lipid biochemical network demonstrates fold differences in 22 root membrane lipid molecular species and 27 glycerolipid molecular species following inoculation with *P. sojae*. Lipid SMILES identifiers were used to calculate PubChem molecular fingerprints and structural similarities. Mapped networks, displaying significance of fold differences in lipids were calculated for all comparisons. Network visualizations display lipids connected based on structural Tanimoto similarity ≥ 0.8 (edge width: 0.8 to 1.0). Node size displays fold differences of means between comparisons and color shows the direction of change compared to control (orange: increased; blue: decreased; gray: inconclusive). Node shape displays lipid structural type (rounded square: membrane lipids; circle: glycerolipids). Lipids displaying significant differences between treatment groups ($p \leq 0.05$) are denoted with black borders

vs. CSI (Fig. 12). Lipid species that changed only within one of these comparisons when considering all other comparisons (root and stem combined) are denoted with dashed outlines and may identify unique markers representative of the biological changes between these groups (Supplemental Table 1).

Discussion

Infectious pathogens usually colonize plant host to obtain nutrients for their own survival and frequently infect plant tissue such as leaves, stems, or roots, facilitating likely spread within the entire plant [66, 67]. In addition, pathogen can particularly colonize cell types like the root epidermis, phloem or cortical cells and spread to vascular cylinder [68]. Although pathogen invasion is normally specific to particular organs, and they gained entry at a distant site [66, 67]. For instance, *R. solanacearum* entered plant root through root surface or root tips, wounds, and secondary emerging points of roots as penetration sites; it then progressed through the cortex, then spread to the vascular cylinder and finally colonized and infected the entire plant [66, 67, 69]. It seems

that, upon contact with the soybean roots, *P. sojae* is recognized by the tolerant cultivar and activated defence responses against pathogen. It is normally accepted that the activation of defence response by host plant could have a major effect on plant growth and development, although the precise underlying strategies are unknown. Besides, the observation that infection of root by *P. sojae* involves morphological changes in certain cell types (Figs. 1). This makes it possible that the overall root development could be changed by the *P. sojae* colonization and infection, either as a result of the activation of anti-fungi responses by tolerant plant or following active control by the pathogen. It was previously demonstrated that pathogens are capable of penetrating intact roots, and move up to the xylem tissue, and they can also penetrate through wounds or natural apertures to older parts of root and hypocotyl tissue [70] (Fig. 2). Plant resistance to pathogen invasion via colonizing the xylem may be correlated to the thickening of the xylem cell walls [71]. However, lipids are critically involved in pathophysiological properties during plant-pathogen interactions, and the alterations in lipid compositions and their functions
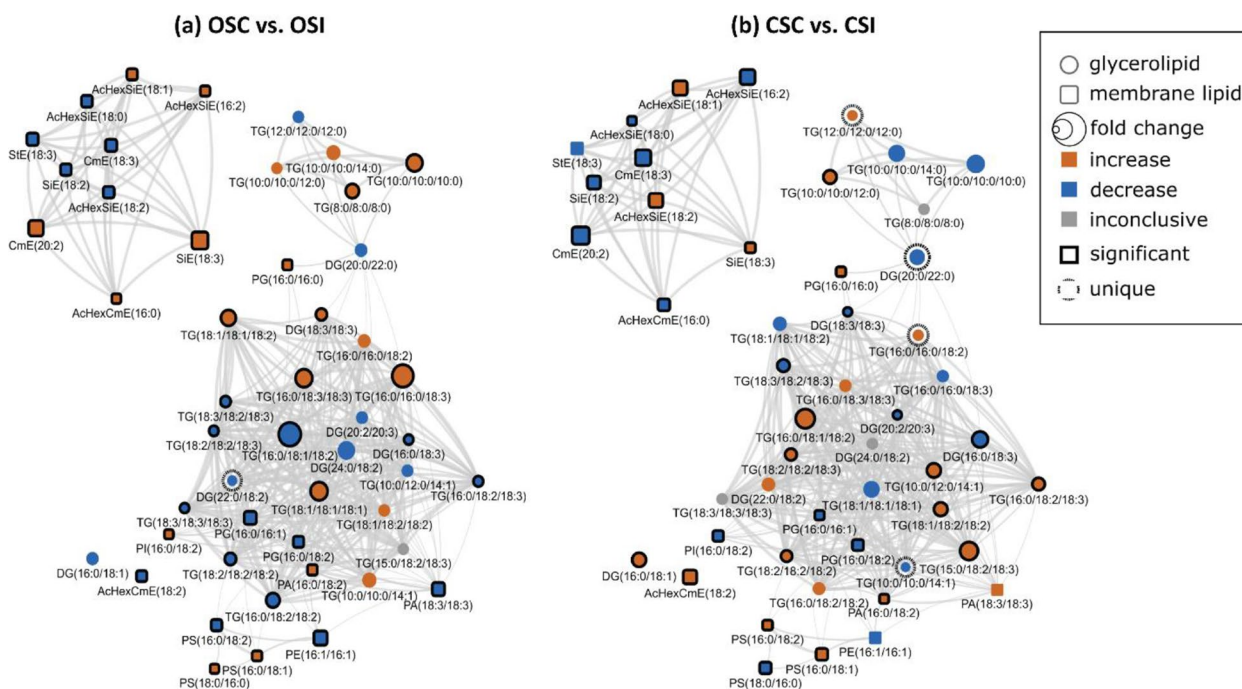

Fig. 11 Lipid structural similarity network displaying differences in stem membrane lipids and glycerolipids in susceptible and tolerant soybean cultivars inoculated with *P. sojae* relative to control plants. **a** Control susceptible soybean cultivar (OSC) versus inoculated (OSI); **b** control tolerant soybean cultivar (CSC) versus inoculated (CSI). The biochemical lipid network demonstrates fold differences in 21 stem membrane lipid molecular species and 28 glycerolipid molecular species following inoculation with *P. sojae*. Lipid SMILES identifiers were used to calculate PubChem molecular fingerprints and structural similarities. Mapped networks, displaying significance of fold differences in lipids were calculated for all comparisons. Network visualizations display lipids connected based on structural Tanimoto similarity ≥ 0.8 (edge width: 0.8 to 1.0). Node size displays fold differences of means between comparisons and color shows the direction of change compared to control (orange: increased; blue: decreased; gray: inconclusive). Node shape displays lipid structural type (rounded square: membrane lipids; circle: glycerolipids). Lipids displaying significant differences between treatment groups ($p \leq 0.05$) are denoted with black borders
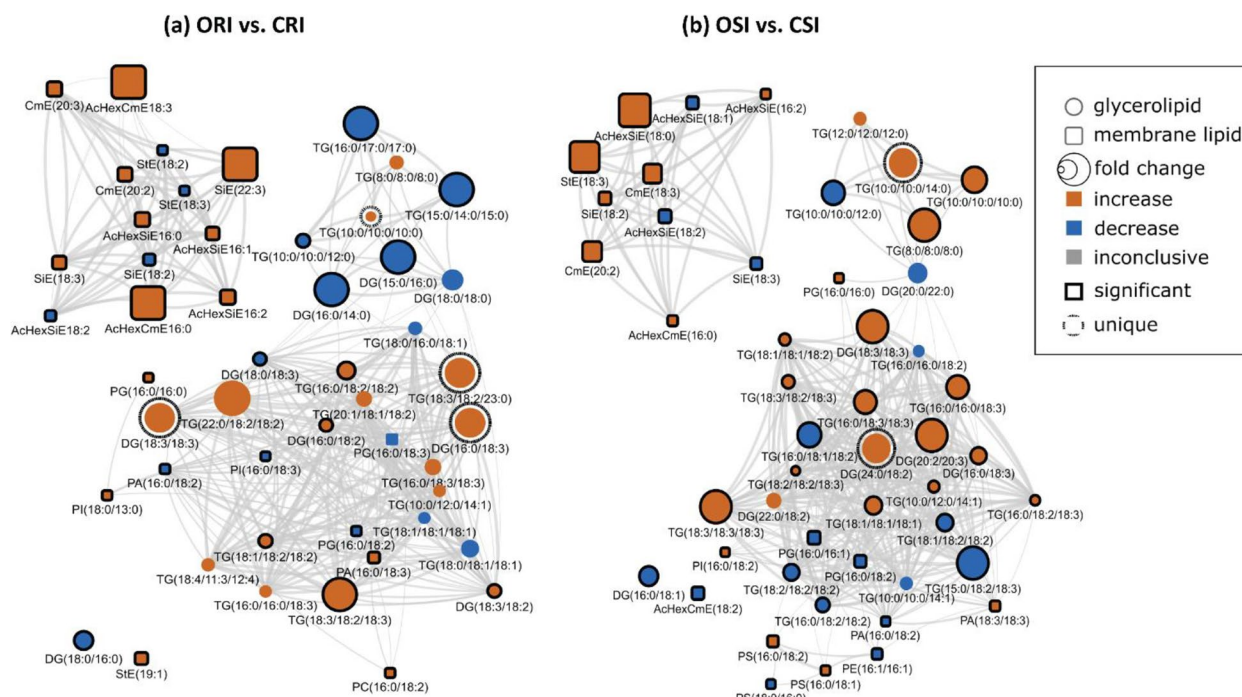
Adigun *et al. BMC Plant Biology*   (2024) 24:154

Page 18 of 26

Fig. 12 Lipid structural similarity network displaying differences in root and stem membrane lipids and glycerolipids in susceptible and tolerant soybean cultivars inoculated with *P. sojae*. **a** Lipids from inoculated root tissue of susceptible (ORI) versus tolerant (CRI) soybean cultivars inoculated with *P. sojae*; and (**b**) Lipids from inoculated stem tissue of susceptible (OSI) versus tolerant (CSI) soybean cultivars inoculated with *P. sojae*. The biochemical lipid network demonstrates fold changes in 22 root membrane lipid molecular species and 27 glycerolipid molecular species, and 21 stem membrane lipid molecular species and 28 glycerolipid molecular species following inoculation with *P. sojae*. Lipid SMILES identifiers were used to calculate PubChem molecular fingerprints and structural similarities. Mapped networks, displaying significance of fold differences in lipids were calculated for all comparisons. Network visualizations display lipids connected based on structural Tanimoto similarity ≥ 0.8 (edge width: 0.8 to 1.0). Node size displays fold differences of means between comparisons and color shows the direction of change compared to control (orange: increased; blue: decreased; gray: inconclusive). Node shape displays lipid structural type (rounded square: membrane lipids; circle: glycerolipids). Lipids displaying significant differences between treatment groups ($p \leq 0.05$) are denoted with black borders

can have significant effects on plant morphology and plant's response to environmental stressors [20, 21]. For instance, lipids enhance the structural integrity of plant cells to involve in cell signaling cascade that activate plant defense responses [20, 21]. This was implicated in the current study where the cell wall of vascular cylinder of the infected tolerant cultivar was observed to be thicker compared to the cell wall of vascular cylinder of the susceptible cultivar when infected with *P. sojae* (Fig. 3). Likewise in plants, crystals may be present and distributed within a single or multiple tissues and varies among plant species though there are no generalities about where crystals can be generated in plants [72] (Figs. 4). It has been generally predicted that the morphology and the distribution of crystals are strictly regulated by plant genes and a specific species will generate a particular type of crystal [72] (Figs. 4). For instance, calcium sulfate crystal and calcium oxalate were found in almost all plant tissues including sclerenchyma, parenchyma and mesophyll, and locations of types of crystals may not or may be tissue-specific [73]. Also, certain functions have been

proposed for crystal formation in plants. For instance, in *Acacia* species, crystals consisting of magnesium, calcium, barium, and strontium are used to regulate the levels of these micronutrients in metabolic partitions in the plants and to avert toxicity [74]. Likewise, biogenic and biological crystals are generally accepted to play some physiological and pathological roles such as support, protection, and defense in plants [20, 21]. Studies have demonstrated that anatomy and physiological functions of vascular cylinder is critically important to plant defense against pathogens [75]. This study demonstrated interesting information about the system of compartmentalization of *P. sojae* in the root of soybean cultivars and recognizes the anatomy of xylem as a major factor of disease resistance. In the root of tolerant cultivar, compartmentalization may be contributory to wall-off *P. sojae* and ensure that the physiological functions and integrity of cellular structures are maintained.

As essential components of cellular membranes, lipids are involved in various physiological roles including as structural components of cellular membranes, cell

signaling, storage of energy, and membrane trafficking. In plants, alterations in lipid composition have been reported in response to pathogenic stress conditions [76]. Biotic stress have been reported to profoundly alter the lipidome in plants [77]. Additionally, Ferrer et al. [78] demonstrated that alterations in the relative composition of PSTs in cellular membranes affect their biophysical properties and hence their physiological functions. The results we describe here indicate significant alterations in lipid mediators in both a tolerant and a susceptible soybean cultivar in response to *P. sojae* infection. Specifically, in the pathogen-treated plants, we observed significantly higher levels of major GPLs and GLs (DGs and TGs) in the tolerant cultivar, whereas StEs and CmEs were found to be higher in quantity in the susceptible cultivar. More interestingly, these classes of lipids varied in a similar manner in the root and stem of each cultivar in response to pathogen infection, which is in line with the literature [77, 79, 80]. For example, similar trends were observed for the lipidome of eggplants (*Solanum melongena*) resistant to Fusarium wilt infection [79], demonstrating the significant difference in the levels of lipid profiling of the susceptible and tolerant eggplants to Fusarium disease and this ensured the essential roles of the lipids in resistance strategy against infection [79]. The increased lipid levels in tolerant cultivars serve as energy stores and provide a buffer to stress; the stored lipids could act as additional energy that keeps the plants from shifting to proteolysis and then cell death [80].

The biosynthesis and lipid composition of cellular membranes play an essential role in the physiological functioning of plants [81]. During growth, plants adapt to adverse stress conditions through the remodelling of lipid membranes resulting from alterations in the fatty acid content and, consequently, the biosynthesis of lipids [81]. Several studies have demonstrated that high levels of lipid remodeling in plant membrane lipids under different adverse conditions result in resistance to environmental stressors [81].

Our results clearly show that there are differences in both membrane and storage lipid mediators in tolerant and susceptible soybean cultivars in response to *P. sojae* infection. For instance, we observed higher levels of 18:2 and 18:3 fatty acyl-enriched phospholipid and sterol molecular species in the membrane lipids of the root and stem from the tolerant cultivar when challenged with the pathogen, in contrast to lower C18:2 and C18:3-enriched molecular species in tissues from the susceptible cultivar (Figs. 6, 7). Several studies have indicated that during pathogen infection, accumulated phospholipid-derived molecular species participate in plant signaling and membrane trafficking, that can induce immunity in plants [36, 37]. For instance, PA is known as a secondary

messenger in plants and its synthesis has been reported to be induced in response to pathogen attack [39, 40]". In line with this, the current study has demonstrated significant accumulation of PA molecular species such as PA16:0/18:2, PG16:0/18:2, PI16:0/18:3, PC16:0/18:2, PS16:0/18:1, PS16:0/18:2, PA18:3/18:3 and PG16:0/16:0 (Figs. 6 and 7) in infected root and stem of tolerant soybean cultivar but no significant changes in infected susceptible cultivar [39, 40]. Similarly, lipid metabolism in guard cells have been attributed to an 18:3 plant species, *Vicia faba* [82]. Guard cell protoplasts from *V. faba* have been demonstrated to generate eukaryotic lipid molecular species [82]. Guard cells are known to contain high level of the triacylglycerols biosynthesized by the eukaryotic lipid metabolic pathway [82]. Recently, it has been established that triacylglycerols stored in guard cells are used to generate adenosine triphosphate required for light-induced stomatal opening.

In contrast, the StEs were significantly higher in the root and stem from the susceptible cultivar challenged with *P. sojae* infection but were significantly lower in the susceptible control plants and in the tolerant cultivar under both treatment conditions (Tables 1, 2; Figs. 6, 7). This is in agreement with a recent study which demonstrated the role of sterols in disease resistance [83]. Stigmasterol ester was identified as a factor of susceptibility in *Arabidopsis*, as inhibition of its biosynthesis resulted in increased resistance to *Pseudomonas syringae* [83, 84]. Following inoculation with pathogenic microorganisms, plants generate an array of metabolic changes that potentially contribute to induce resistance or even enhance susceptibility. In this study, we observed that accumulation of stigmasterol is an important plant metabolic process that occurs upon pathogen infection in soybean-*P sojae* pathosystem. For instance, we noticed the significant accumulation of StE 19:1, AcHexCmE 18:3, CmE20:2, AcHexSiE16:0, AcHexSiE18:1, SiE18:3, AcHexSiE16:2 and AcHexCmE16:0 in infected root and stem of susceptible soybean cultivar but no significant changes in infected tolerant cultivar (Figs. 6 and 7). This is consistent with previous reports showing β-sitosterol and stigmasterol accumulation promoted *Arabidopsis* susceptibility to *P. syringae* [84], through the enzyme CYP710A1. Stigmasterol is biosynthesized from β-sitosterol via cytochrome P450 CYP710A1 [84]. For instance, Arabidopsis *cyp710A1* mutant lines compromised in pathogen-inducible expression of C22 desaturase and associated stigmasterol accumulation are highly resistant to both virulent and avirulent *P. syringae* strains compared to the wild-type plants, and exogenous utilization of stigmasterol impaired this resistance phenotype. Thus induced sterol desaturation in susceptible soybean cultivar appears to favours pathogen multiplication and

Adigun *et al. BMC Plant Biology*   (2024) 24:154

Page 20 of 26

plant susceptibility [84]. The formation of stigmasterol in leaves is induced by recognition of bacterial pathogen-associated molecular patterns and synthesis of reactive oxygen species, but is independent of the jasmonic acid, salicylic acid or ethylene-associated signalling pathways [84]. Through analysis of mutants and application of exogenous sterol, it was demonstrated that an increase in the ratio of stigmasterol to β-sterol in leaves reduces specific defence responses in *Arabidopsis*, and consequently makes the plants more susceptible to *P. syringae* [4, 48]. These were in line with the results obtained in this study, and these modes of action may account for the higher resistance of the tolerant cultivar to pathogen infection.

Pathogenic fungi can secrete various extracellular enzymes that are involved in pathogenicity [85]. For example, secreted lipases from fungal pathogens are involved in the penetration of plant barriers such as the wax cuticle. Similarly, fungal lipases are capable of degrading storage and signaling lipids via the release of secondary messengers. The significant decrease in the TG molecular species such as TG 18:1/18:1/18:1, TG 18:0/18:0/18:0, TG 18:0/16:0/18:1, TG 16:0/18:3/18:3, TG 16:0/16:0/18:3, TG 10:0/12:0/14:1 and TG 10:0/10:0/100 (Figs. 8 and 9) in the soybean susceptible cultivar in this study could be a result of increased lipase activity during infection. For instance, lipases hydrolyze carboxyl esters in TGs liberating fatty acids and glycerol [86]. This agrees with the fact that lipases appear to function as virulent factors in plant pathogens. More interestingly, the tolerant cultivar demonstrated significantly higher DG levels such as DG15:0/16:0, DG16:0/14:0, DG18:0/16:0, DG18:0/18:0 and DG16:0/18:1 (Figs. 8 and 9) in response to pathogen infection, but there was no observed difference in TG levels. DGs are primarily derived either from TGs through TG lipases or from PAs by phospholipase activity [79, 87]". These findings suggest that soybean root lipidome and metabolism is remodeled in response to pathogen colonization and infection and appears to be part of the successful strategy used by the host in this pathosystem to survive pathogen attack. The lipid biochemical network demonstrated significant alterations in lipid mediators in both cultivars in response to *P. sojae* infection. The head group and FA composition of complex lipids are a useful proxy for localization and biological function [88]. Networks display increased density in connectivity between biochemically related groups of lipids and the lipid biosynthesis metabolism pathway in the tolerant soybean cultivar as defense response to pathogen inversion. Generally, there is dearth of information on the role of lipid mediators in determining either incompatible or compatible interactions in the soybean-*P sojae* pathosystem during host–pathogen interaction. The unique biomarkers

between the susceptible and tolerant cultivars including the production of DG molecular species, which was well pronounced in tolerant cultivar than susceptible (Figs. 10, 11 and 12). Studies have demonstrated that signaling enzymes, diacylglycerol kinases (DGKs) play important roles in response to biotic stress by phosphorylating DG to synthesis PA (Fig. 13) and both PA and DG are lipid mediators during physiological process [89]. Our findings from this study demonstrate that lipid mediators and signalling possibly involving DG could play a significant role in pathogen resistance in the tolerant soybean cultivar. Also, DG signally related to TG hydrolysis which was differentially demonstrated between susceptible and tolerant soybean cultivars when challenged with pathogen (Figs. 8 and 9). Study has demonstrated that TG is accumulated in plant tissues due to TG turnover, as a result of disruption of SUGAR-DEPENDENT1, a cytosolic lipase accountable for TG hydrolysis in lipid droplets into free FAs and DG and consequently enhance TG accumulation in plant tissues [90]. Fan et al. [91] demonstrated that TG accumulation plays important role, thus buffering homeostasis of lipid and protecting plant cells against lipotoxic death as a results FA overload and can be as a remodeling of robust membrane in response to stresses. Phytosterols also known to play important role in plant innate immunity against pathogen attack [48]. However, the odd chain FAs that appear in the lipid profile are usually and maybe fungal origin and they are mainly unique to the infected soybean [92]. The extracted ion chromatograms of *the odd chain FAs* are shown in Fig. S1 and MS^2 spectrum of *m/z* 856.73 identified as TG 15:0/18:2/18:3 $[M+NH_4]^+$ is depicted in Fig. S2.

Lipid biosynthesis in soybean cultivars follow common routes where FAs are generated from plastid, transported to the endoplasmic reticulum (ED) [38], which starts with the addition of fatty acyl-CoA leading to biosynthesis of lysophosphatidic acid (LPA) and the reaction is catalyzed by glycerol phosphate acyltransferase (GPAT) and is a rate limiting-step for PA biosynthesis. In ED, PA biosynthesis occurs by addition of fatty acyl-CoA to LPA via lysophosphatidic acid acyltransferase (LPAAT) to form central precursor PA by which several GPLs are synthesized (Fig. 13). The first step in GPLs biosynthesis involves the hydrolysis of the phosphate group from PA to generate DG by phosphatidic acid phosphatase (PAP). The resulting DG is later phosphorylated by DGKs to PA, which is subsequently reused in biosynthesis of GPLs. Also, DG acts as a precursor for biosynthesis of primary form of storage energy, TG [93]. The isopentenyl diphosphate (IPP) and dimethylallyl pyrophosphate (DMAPP) generated via cytosolic mevalonate (MVA) pathway are primarily used for the biosynthesis of phytosterols [94, 95]. Our results
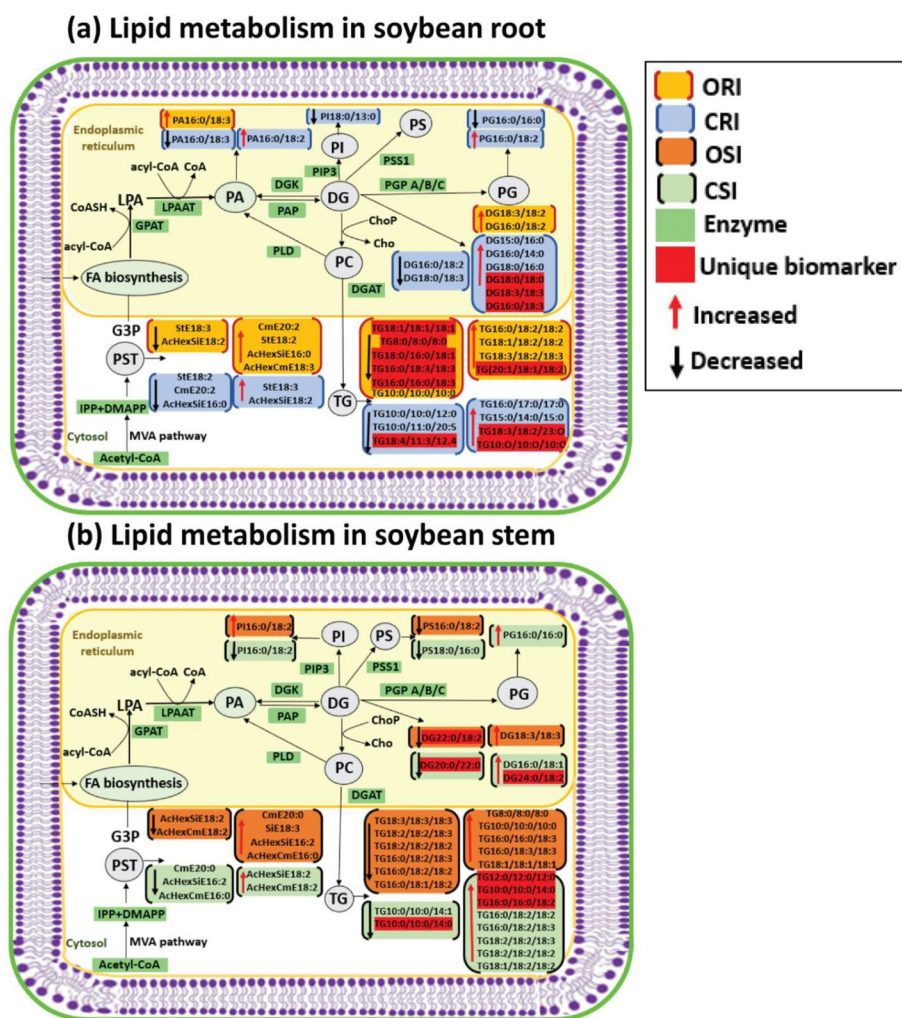
Fig. 13 Proposed lipid metabolism pathways suggesting the mechanism that maybe associated with the altered lipid mediators and disease tolerance or susceptibility in soybean cultivars (OX760-6 and Conrad) following inoculation with *P. sojae*. **a** The most significantly altered root lipids in soybean cultivars in response to infection with *P.sojae*; and (**b**) The most significantly altered stem lipids in soybean cultivars in response to *P. sojae* infection. In the Kennedy pathway fatty acyl-CoA and coenzyme A begins with the sequential acylation of GPATs and LPAATs utilizing fatty acyl-CoA to biosynthesis the central precursor PA through which other downstream GPLs are produced. GLPs are produced through hydrolysis of the phosphate group in PA, and this PA then dephosphorylated through PAP to generate DG. The DG acts as a precursor for biosynthesis of TG via DGAT or PDAT transferring the sn-2 fatty acyl group from GPLs to DG, producing TG. Biosynthesis of IPP and DMAPP through mevalonate (MVA) pathway, and they act as precursors for phytosterol synthesis. The altered lipidome observed in this study suggest DG and PA mediated lipid signalling impacting phytosterol anabolism appears to be the strategy used by tolerant soybean cultivars to successfully limit infection and colonization by *P.sojae*. The following molecular species are suggested as unique lipid biomarkers in the ORI vs CRI and CSI vs OSI networks that could potentially discriminate tolerance interations in the soybean-*P.sojae* pathosystem: TG(18:3/18:2/23:0), TG(10:0/10:0/10:0), TG(10:0/10:0/14:0), DG(18:3/18:3), DG(16:0/18:3) and DG(24:0/18:2). PLD = phospholipase D, DGK = diacylglycerol kinase, LPAAT = lysophosphatidic acid acylteransferase, PAP = phosphatic acid phosphatase, G3P = glycerol-3-phosphate, DGAT = diacylglycerol acyltranferase, GPAT = Glycerol-3-phosphate acyltransferase, PDAT = phospholipid:diacylglycerol acyltransferases, PSS1 = phosphatidylserine synthase-1, PGP = glycerol-3-phosphate phosphatase, PAP = phosphatidic acid phosphatase, IPP = isopentenyl pyrophosphate, DMAPP = dimethylallyl pyrophosphate, MVA = mevalonic acid, PIP3 = 1-phosphatidylinositol-4-phosphate 5-kinase, CoASH = coenzyme A, Chop = cholinephosphotransferase and cho = choline. ORI = root of susceptible inoculated, CRI = root of tolerant inoculated, OSI = stem of susceptible inoculated, CSI = stem of tolerant inoculated, GPLs = glycerophospholipids, GLs = glycerolipids, LPA = lysophosphatidic, PA = phosphatidic acid, PC = phosphatidylcholine, PG = phosphatidyl glycerol, PI = phosphatidylinositol, PS = phosphatidylserine, DG = diacylglycerol, TG = triacylglycerol and PST = phytosterols

demonstrate novel information about pathogen-stress responses in the root and stem of both soybean cultivars, which can be put within the broad context of plant lipid mediators. The metabolic pathway of relative abundance of GPL, PST and GL biosynthesized in the root and stem of the susceptible and tolerant soybean cultivars when

challenged with *P. sojae* are demonstrated in Fig. 13. These lipid classes could be used as biomarkers for disease resistance or susceptibility by soybean cultivars. Based on our understanding, this is the first report of lipid alteration in soybean root and stem in response to *P. sojae* infection.

Conclusions

Our results reported the chemical, physical and morphological changes in the roots of both susceptible and tolerant soybean cultivars challenged with *P. sojae* and to further improve our understanding of the mechanism of infection in soybean-*P. sojae* interaction. It also demonstrated promise for a novel mechanism to develop soybean cultivars for wide spectrum disease susceptibility or resistance by manipulating plant lipid levels. Both soybean cultivars altered lipid biosynthesis upon infection by *P. sojae*. Induced accumulation of stigmasterol, and total increase in the ratio of stigmasterol to β-sitosterol in the susceptible soybean cultivar favoured pathogen multiplication and then improved disease susceptibility whereas induced accumulation and overall increase in GPLs (PA and PG) and GLs (DG and TG) in tolerant soybean cultivar enhanced plant immunity against pathogen. Glycerophospholipids strengthen the cellular membrane and protect plant cells from various infections while DGs mainly act as signalling molecules during response to various environmental stresses. The altered lipidome observed in this study suggest DG and PA mediated lipid signalling impacting phytosterol anabolism appears to be the strategy used by tolerant soybean cultivars to successfully limit infection and colonization by *P. sojae*. The following molecular species are suggested as unique lipid biomarkers in the networks that could potentially discriminate tolerance interactions in the soybean-*P. sojae* pathosystem: ORC vs ORI {TG(20:1/18:1/18:2), TG(18:1/18:1/18:1), TG(8:0/8:0/8:0), TG(18:0/16:0/18:1), TG(16:0/18:3/18:3), TG(16:0/16:0/18:3)}; CRC vs CRI {TG(18:4/11:3/12:4), DG18:0/18:0}; OSC vs OSI {DG22:0/18:2}; CSC vs CSI {TG(12:0/12:0/12:0), TG(16:0/16:0/18:2), TG(10:0/10:0/14:0), DG20:0/22:0}; ORI vs CRI {TG(18:3/18:2/23:0, TG(10:0/10:0/10:0), DG(18:3/18:3), DG(16:0/18:3)} and CSI vs OSI {TG(10:0/10:0/14:0), DG(24:0/18:2)}. Therefore, morphological and chemical changes appears to play a critical role in disease resistance by tolerant plants, and could be used to potentially develop a novel strategy to engineer soybean crop cultivars with wide-ranging disease tolerance against *P.sojae* in this pathosystem. We hope this work will stimulate further studies to better understand the exact roles plant lipids play in membrane permeability and as signaling molecules mediating plant immunity.

Methods

Plant growth and inoculation method

A virulent strain of *P. sojae* race 2 (strain P6497) obtained from the London Research and Development Center, Agriculture and Agri-Food Canada (AAFC-LRDC; London, ON, Canada) was used as inoculum. The oomycete was cultured and maintained aseptically for 8 days on 26% V8-juice agar (8400 mg agar, 1600 mg $CaCO_3$, 156 mL V8-juice [Campbell Soup Company, Toronto, ON, Canada], and 440 mL of distilled water). Seeds of soybean cultivars Conrad (*P. sojae*-tolerant) and OX760-6 (*P. sojae*-susceptible) were obtained from AAFC-LRDC (London, ON, Canada). The seeds were surface disinfected for 5 min using 0.5% sodium hypochlorite (Commercial Javex Bleach; Clorox Co., Brampton, Ontario, Canada) and rinsed with distilled water several times. The seeds were then soaked for 12 h in distilled water before seeding. Agar disks containing *P. sojae (isolate* P6497) were carefully cut from each agar plate using an empty cup as a clamp. Each disk was fitted into the bottom of empty wax-paper cups with a top diameter of 8.5 cm and 15.0 cm deep (Merchants Paper Company, Windsor, ON, Canada) and overlaid with medium-grade vermiculite. Drainage holes were created in the bottom of the cups. The imbibed seeds were planted in the medium-grade vermiculite. Six soybean seedlings from each cultivar were inoculated with *P. sojae* and another six from each cultivar were mock-inoculated (sterile V8-juice agar disks without any *P. sojae* culture) in a cup as the control. The plants were then grown and inoculated using agar disk placed in the bottom of the cups for 10 days and seedlings (10 days old) used for subsequent analysis and lab experimentation. Susceptible plants started showing symptom of infection at 6 days after growth in the medium containing the agar disks [7, 8]. The plant growth experiment was performed in a growth chamber (Biochambers MB, Canada) at Grenfell Campus, Memorial University of Newfoundland, under controlled growth conditions of 16 h light at 25 °C and 8 h dark at 20 °C, and relative humidity of 60%. Seedlings were watered daily 4 days after seeding with one-quarter-strength Knop's solution [8]. The whole seedlings were collected 10 days after growth and stored at -80 °C until further analysis.

Preparation of samples for scanning electron microscopy

Soybean roots were collected from both non-inoculated (control) and inoculated plants of susceptible and tolerant soybean cultivars. The samples were rinsed with distilled water before further processing. Free-hand cross sections of the root were cut using a razor blade to a length of approximately 5 mm. Thin sections were mounted to aluminum stubs using colloidal graphite

adhesive (Permatex, Canada, Incorporated). The samples were exposed to a temperature of -4.9 °C on a Peltier cooling stage to minimize differences in structure, while in the vacuum chamber. The images of the samples were collected using an environmental scanning electron microscope (ThermoFisher Quattro S with ESEM), to study the morphological properties of roots infected with *P. sojae*. High-resolution images were collected from 9–10 mm to 5–100 μm (magnification 788-8000X with the pressure 50–428 Pa).

Method of lipid extraction

Soybean seedlings prepared as above were incubated in boiling isopropanol for 10 min. Lipid extraction was conducted by weighing 100 mg each of root and stem from each sample type, and 1 mL MeOH containing 0.01% butylated hydroxytoluene was added to each sample. Four replications of each combination of treatment (inoculated or control), cultivar (susceptible or tolerant), and tissue (root or stem) combination were performed. The tissues were then homogenized using a probe tissue homogenizer until completely dissolved. Following homogenization, 800 μL water and 1000 μL chloroform were added along with PC 14:0/14:0 as internal standard. Each sample was thoroughly vortexed and centrifuged at 3000 rpm for 15 min at room temperature. The organic layers were transferred to pre-weighed 4 mL glass vials with PTFE-lined caps (VWR, Mississauga, Canada). The samples were then dried under a gentle stream of nitrogen and the sample vials reweighed to determine the quantity of recovered lipids. The recovered lipids from each sample were re-suspended in 1000 μL solvent (2:1 v/v chloroform: methanol) and stored at -20 °C until lipid analysis using ultra high-performance liquid chromatography coupled to heated electrospray ionization high resolution accurate mass tandem mass spectrometry (UHPLC- C30RP-HESI-HRAM-MS/MS).

Lipid analysis using UHPLC-C30RP-HESI-HRAM-MS/MS

The method of lipid analysis was as described previously [32, 96, 97]. Lipids extracted from the soybean roots and stems were separated using an Accucore C30 reverse phase (C30RP) column (150×2 mm I.D., particle size: 2.6 μm, pore diameter: 150 Å; ThermoFisher Scientific, ON, Canada) applying the following solvent system: Solvent A (40: 60 v/v H_2O and acetonitrile), and Solvent B (1:10: 90 v/v/v water: acetonitrile: isopropanol). Both solvents A and B consisting of 0.1% formic acid and 10 mM ammonium formate. The conditions for the separation using UHPLC-C30RP were as follows: oven temperature of 30 °C, flow rate of 0.2 mL/min, and 10 μL of the lipid mixture suspended in 1: 2 v/v methanol: chloroform was injected into the instrument. The system gradient used for the separation of lipid classes and molecular species were: 30% solvent B for 3 min; solvent B increased over 5 min to 43%, then increased in 1 min to 50% B and to 90% B over 9 min; and from 90 to 99% B over 8 min; and finally maintained at 99% B for 4 min. The column was re-equilibrated to 70% solvent A for 5 min to re-establish the starting conditions before injection of each new sample. Lipid analyses were performed using a Q-Exactive Orbitrap high-resolution accurate mass tandem mass spectrometer (Thermo-Scientific, Berkeley, CA, USA) coupled with an automated Dionex Ulti-Mate 3000 UHPLC system controlled by Chromeleon 6.8 SR13 (Dionex Corporation, Part of Thermo Fisher Scientific) software. Full-scan HESI-MS and MS/MS acquisitions were performed in positive mode of the Q-Exactive Orbitrap mass spectrometer. The following parameters were used for the Orbitrap mass spectrometry techniques: auxiliary gas of 2; sheath gas of 40; capillary temperature of 300 °C; ion spray voltage of 3.2 kV; S-lens RF of 30 V; full-scan mode at a resolution of 70,000 m/z; mass range of 200–2000 m/z; top-20 data dependent MS/MS acquisitions at a resolution of 35,000 m/z; and injection time of 35 min; automatic gain control target of 5e5; isolation window of 1 m/z; collision energy of 35 (arbitrary unit). The external calibration of instrument was performed to 1 ppm using ESI positive and negative calibration solutions (Thermo Scientific, Berkeley CA, USA). Mixtures of lipid standards were used to optimize tune parameters (Avanti Polar Lipids, Alabaster, AL, USA) in both positive and negative ion modes. Identification and semi-quantification of the classes of lipids and lipid molecular species present in the root and stem of both soybean cultivars (OX760-6 and Conrad) were performed using LipidSearch version 4.1 (Mitsui Knowledge Industry, Tokyo, Japan) and the parameters adopted for identification in LipidSearch were: target database of Q-Exactive; product tolerance of 5 ppm; precursor tolerance of 5 ppm; Quan m/z tolerance of ± 5 ppm; product ion threshold of 5%; m-score threshold of 2; Quan retention time range of ± 1 min; use of all isomer filter; ID quality filters A, B, and C; and $[M+NH_4]^+$ adduct ions for positive ion mode. Following identification, the observed lipid classes and lipid molecular species were merged and aligned according to the parameters established in our previous report [98].

Lipid biochemical network mapping

To better understand how soybean cultivars that are tolerant and susceptible to *P. sojae* modulate their membrane lipid mediators as part of the plant defense response strategy during infection and colonization, lipids that changed significantly between treatments were visualized within lipid structural similarity and

Adigun *et al. BMC Plant Biology*   (2024) 24:154

Page 24 of 26

implied activity networks. Lipid SMILES identifiers obtained from lipid map were used to calculate PubChem molecular fingerprints describing lipids' sub structures [99]. Connections between lipids were defined based on Tanimoto similarity ≥ 0.8 between fingerprints. Significance of fold changes in lipid expression levels were mapped to network node attributes and displayed using Cytoscape [100, 101]. Node size was used to represent fold changes of means between treatments, and colors indicated the direction of change compared to control (orange = increased; blue = decreased; gray = inconclusive) in the lipid network map generated. Node shape was used to indicate lipid structural type (rounded square = membrane lipids; circle = neutral lipids). Lipids displaying significant differences between treatment groups ($p \leq 0.05$) were denoted with black borders.

Statistical analysis

To determine the effects of pathogen infection on lipid composition of the root and stem of susceptible and tolerant cultivars, multivariate analyses including partial least square discriminant analysis (PLS-DA), and heat map were performed to group the treatments based on similarity. Analysis of variance (ANOVA) was next performed to determine whether the groups were significantly different between treatments using XLSTAT (2017 Premium edition, Addinsoft, Paris, France). Where significant differences were observed, the means were compared with Fisher's Least Significant Difference (LSD), $\alpha = 0.05$. Figures were prepared with SigmaPlot 13.0 (Systat Software Inc., San Jose, CA).

Supplementary Information

The online version contains supplementary material available at https://doi.org/10.1186/s12870-024-04808-z.

Supplementary Material 1.

Supplementary Material 2.

Supplementary Material 3.

Supplementary Material 4.

Supplementary Material 5.

Supplementary Material 6.

Supplementary Material 7.

Supplementary Material 8.

Supplementary Material 9.

Supplementary Material 10.

Supplementary Material 11.

Supplementary Material 12.

Supplementary Material 13.

Supplementary Material 14.

Availability of data and materials

All data generated or analysed during this study are included in this published article [and its Supplementary information files].

Declarations

Ethics approval and consent to participate

We did not collect the plant materials used in this study. The materials were supplied by Agriculture Agri-Food Canada and formal identification was not carried out and there is no voucher specimen and deposition number for the seeds. Experimental research and field studies on plants (cultivated), was complied with relevant institutional, national, and international guidelines and legislation. All methods were performed in accordance with the relevant guidelines and regulations.

The plant material used in this study were not a rare/ wild type and a voucher specimen of this material was not deposited in a publicly available herbarium.

Consent for publication

Not applicable.

Competing interests

The authors declare no competing interest.

References

1. Adigun OA, et al. Phyto-oxylipin mediated plant immune response to colonization and infection in the soybean-Phytophthora sojae pathosystem. Front Plant Sci. 2023;14:1141823.
2. Wudil AH, et al. Reversing years for global food security: A review of the food security situation in Sub-Saharan Africa (SSA). Int J Environ Res Public Health. 2022;19(22):14836.
3. Adigun OA, et al. Recent advances in bio-chemical, molecular and physiological aspects of membrane lipid derivatives in plant pathology. Plant Cell Environ. 2020;44(1):1–16.
4. Ali U, et al. Emerging roles of sphingolipid signaling in plant response to biotic and abiotic stresses. Mol Plant. 2018;11(11):1328–43.
5. Amos RA, Mohnen D. Critical review of plant cell wall matrix polysaccharide glycosyltransferase activities verified by heterologous protein expression. Front Plant Sci. 2019;10:915.
6. Bates PD, Browse J. The significance of different diacylglycerol synthesis pathways on plant oil composition and bioengineering. Front Plant Sci. 2012;3:147.
7. Berkey R, Bendigeri D, Xiao S. Sphingolipids and plant defense/disease: the "death" connection and beyond. Front Plant Sci. 2012;3:68–68.
8. Boller T, Felix G. A renaissance of elicitors: perception of microbe-associated molecular patterns and danger signals by pattern-recognition receptors. Annu Rev Plant Biol. 2009;60:379–406.

9. Boutté Y, Jaillais Y. Metabolic cellular communications: feedback mechanisms between membrane lipid homeostasis and plant development. Dev Cell. 2020;54(2):171–82.
10. Brackin R, et al. Roots-eye view: using microdialysis and microCT to non-destructively map root nutrient depletion and accumulation zones. Plant Cell Environ. 2017;40(12):3135–42.
11. Caffall KH, Mohnen D. The structure, function, and biosynthesis of plant cell wall pectic polysaccharides. Carbohydr Res. 2009;344(14):1879–900.
12. Canonne J, Froidure-Nicolas S, Rivas S. Phospholipases in action during plant defense signaling. Plant Signal Behav. 2011;6(1):13–8.
13. Casares D, Escribá PV, Rosselló CA. Membrane lipid composition: effect on membrane and organelle structure, function and compartmentalization and therapeutic avenues. Int J Mol Sci. 2019;20(9):2167.
14. Cassim AM, et al. Plant lipids: key players of plasma membrane organization and function. Prog Lipid Res. 2019;73:1–27.
15. Chapman KD, Dyer JM, Mullen RT. Biogenesis and functions of lipid droplets in plants: thematic review series: lipid droplet synthesis and metabolism: from yeast to man. J Lipid Res. 2012;53(2):215–26.
16. Christensen SA, Kolomiets MV. The lipid language of plant-fungal interactions. Fungal Genet Biol. 2011;48(1):4–14.
17. Cuéllar-Cruz M, et al. Biocrystals in plants: a short review on biomineralization processes and the role of phototropins into the uptake of calcium. Crystals. 2020;10(7):591.
18. Dangl JL, Horvath DM, Staskawicz BJ. Pivoting the plant immune system from dissection to deployment. Science. 2013;341(6147):746–51.
19. Digonnet C, et al. Deciphering the route of Ralstonia solanacearum colonization in Arabidopsis thaliana roots during a compatible interaction: focus at the plant cell wall. Planta. 2012;236(5):1419–31.
20. Ding L-N, et al. Plant disease resistance-related signaling pathways: recent progress and future prospects. Int J Mol Sci. 2022;23(24):16200.
21. Dong W, et al. Does diacylglycerol serve as a signaling molecule in plants? Plant Signal Behav. 2012;7(4):472–5.
22. Dorrance AE, McClure SA, St SK. Martin, effect of partial resistance on Phytophthora stem rot incidence and yield of soybean in Ohio. Plant Dis. 2003;87(3):308–12.
23. Downie HF, et al. Challenges and opportunities for quantifying roots and rhizosphere interactions through imaging and image analysis. Plant Cell Environ. 2015;38(7):1213–32.
24. Elmore JM, Coaker G. The role of the plasma membrane H+-ATPase in plant–microbe interactions. Mol Plant. 2011;4(3):416–27.
25. Fan J, Yu L, Xu C. A central role for triacylglycerol in membrane lipid breakdown, fatty acid β-Oxidation, and plant survival under extended darkness. Plant Physiol. 2017;174(3):1517–30.
26. Ferrer A, et al. Emerging roles for conjugated sterols in plants. Prog Lipid Res. 2017;67:27–37.
27. Fletcher J, et al. Plant pathogen forensics: capabilities, needs, and recommendations. Microbiol Mol Biol Rev. 2006;70(2):450–71.
28. Franceschi VR, Nakata PA. Calcium oxalate in plants: formation and function. Annu Rev Plant Biol. 2005;56:41–71.
29. Gao QM, et al. Mono- and digalactosyldiacylglycerol lipids function nonredundantly to regulate systemic acquired resistance in plants. Cell Rep. 2014;9(5):1681–91.
30. Garay LA, Boundy-Mills KL, German JB. Accumulation of high-value lipids in single-cell microorganisms: a mechanistic approach and future perspectives. J Agric Food Chem. 2014;62(13):2709–27.
31. Goufo P, Cortez I. A lipidomic analysis of leaves of esca-affected grapevine suggests a role for galactolipids in the defense response and appearance of foliar symptoms. Biology. 2020;9(9):268.
32. Grapov D, Wanichthanarak K, Fiehn O. MetaMapR: pathway independent metabolomic network analysis incorporating unknowns. Bioinformatics (Oxford, England). 2015;31(16):2757–60.
33. Griebel T, Zeier J. A role for β-sitosterol to stigmasterol conversion in plant–pathogen interactions. Plant J. 2010;63(2):254–68.
34. Guha R. Chemical informatics functionality in R. J Stat Softw. 2007;18(5):1–16.
35. Hall C, Heath R, Guest D. Rapid and intense accumulation of terpenoid phytoalexins in infected xylem tissues of cotton (Gossypium hirsutum) resistant to Fusarium oxysporum f.sp. vasinfectum. Physiol Mol Plant Pathol. 2011;76:182–8.
36. Hannun YA, Obeid LM. Sphingolipids and their metabolism in physiology and disease. Nat Rev Mol Cell Biol. 2018;19(3):175–91.
37. He H, et al. Morphologies and elemental compositions of calcium crystals in phyllodes and branchlets of Acacia robeorum (Leguminosae: Mimosoideae). Ann Bot. 2012;109(5):887–96.
38. He M, et al. Plant unsaturated fatty acids: Biosynthesis and regulation. Front Plant Sci. 2020;11:390.
39. Heung LJ, Luberto C, Del Poeta M. Role of sphingolipids in microbial pathogenesis. Infect Immun. 2006;74(1):28–39.
40. Hudgins JW, Krekling T, Franceschi VR. Distribution of calcium oxalate crystals in the secondary phloem of conifers: a constitutive defense mechanism? New Phytol. 2003;159(3):677–90.
41. Ilarslan H, Palmer RG, Horner HT. Calcium oxalate crystals in developing seeds of soybean. Ann Bot. 2001;88(2):243–57.
42. Kelly AA, et al. The sugar-dependent1 lipase limits triacylglycerol accumulation in vegetative tissues of Arabidopsis. Plant Physiol. 2013;162(3):1282–9.
43. Kelly K, Jacobs R, F.a.N.S.L. Department of Agricultural, University of Alberta, Edmonton, AB, Canada, Editor.
44. Kim HU. Lipid metabolism in plants. Plants (Basel, Switzerland). 2020;9(7):871.
45. Kim D, et al. Lipid profiles in wheat cultivars resistant and susceptible to tan spot and the effect of disease on the profiles. Phytopathology. 2013;103(1):74–80.
46. Kopischke M, et al. Impaired sterol ester synthesis alters the response of Arabidopsis thaliana to Phytophthora infestans. Plant J. 2013;73(3):456–68.
47. Laxalt AM, Munnik T. Phospholipid signalling in plant defence. Curr Opin Plant Biol. 2002;5(4):332–8.
48. Lim G-H, et al. Fatty acid– and lipid-mediated signaling in plant defense. Annu Rev Phytopathol. 2017;55(1):505–36.
49. Ling S, et al. Biopolymer nanofibrils: structure, modeling, preparation, and applications. Prog Polym Sci. 2018;85:1–56.
50. Lohr M, Schwender J, Polle JEW. Isoprenoid biosynthesis in eukaryotic phototrophs: a spotlight on algae. Plant Sci. 2012;185–186:9–22.
51. Martínez E, et al. Oxylipins mediate cell-to-cell communication in Pseudomonas aeruginosa. Communications Biology. 2019;2(1):66.
52. Matemilola S, Elegbede I. The challenges of food security in Nigeria. Open Access Library Journal. 2017;04(12):22.
53. Mc Carthy U, et al. Global food security – issues, challenges and technological solutions. Trends Food Sci Technol. 2018;77:11–20.
54. Morris H, et al. The parenchyma of secondary xylem and its critical role in tree defense against fungal decay in relation to the CODIT model. Front Plant Sci. 2016;7:1665.
55. Murphy DJ. The dynamic roles of intracellular lipid droplets: from archaea to mammals. Protoplasma. 2012;249(3):541–85.
56. Nadeem M, et al. Adaptation strategies of forage soybeans cultivated on acidic soils under cool climate to produce high quality forage. Plant Sci. 2019;283:278–89.
57. Nadeem M, et al. The soybean root membrane lipids and forage quality data in response to field cultivation on agricultural podzols in boreal climates. Data Brief. 2019;25:104055.
58. Nadeem M, et al. Root membrane lipids as potential biomarkers to discriminate silage-corn genotypes cultivated on podzolic soils in boreal climate. Physiol Plant. 2020;170(3):440–50.
59. Naguib DM. Comparative lipid profiling for studying resistance mechanism against Fusarium wilt. Physiol Mol Plant Pathol. 2019;108:101421.
60. Nguema-Ona E, et al. Cell wall O-glycoproteins and N-glycoproteins: aspects of biosynthesis and function. Front Plant Sci. 2014;5:499–499.
61. Nurul Islam M, Chambers JP, Ng CKY. Lipid profiling of the model temperate grass, Brachypodium distachyon. Metabolomics. 2012;8(4):598–613.
62. Okubara P, Paulitz T. Root defense responses to fungal pathogens: a molecular perspective. 2006. p. 215–226.
63. Pauly M, Keegstra K. Cell-wall carbohydrates and their modification as a resource for biofuels. Plant J. 2008;54(4):559–68.
64. Pham TH, et al. Targeting modified lipids during routine lipidomics analysis using HILIC and C30 reverse phase liquid chromatography coupled to mass spectrometry. Sci Rep. 2019;9(1):5048.

Adigun *et al. BMC Plant Biology*   (2024) 24:154

Page 26 of 26

65. Pham TH, et al. Big game cervid meat as a potential good source of plasmalogens for functional foods. J Food Compos Anal. 2021;96:103724.
66. Raffaele S, Leger A, Roby D. Very long chain fatty acid and lipid signaling in the response of plants to pathogens. Plant Signal Behav. 2009;4(2):94–9.
67. Ranathunge K, et al. Soybean root suberin and partial resistance to root rot caused by Phytophthora sojae. Phytopathology. 2008;98(11):1179–89.
68. Ravipati S, et al. Plasma lipid biomarker signatures in squamous carcinoma and adenocarcinoma lung cancer patients. Metabolomics. 2015;11(6):1600–11.
69. Reszczyńska E, Hanaka A. Lipids composition in plant membranes. Cell Biochem Biophys. 2020;78(4):401–14.
70. Řezanka T, Kolouchová I, Sigler K. Precursor directed biosynthesis of odd-numbered fatty acids by different yeasts. Folia Microbiol. 2015;60(5):457–64.
71. Rich MK, Schorderet M, Reinhardt D. The role of the cell wall compartment in mutualistic symbioses of plants. Front Plant Sci. 2014;5:238.
72. Rocha J, et al. Do galactolipid synthases play a key role in the biogenesis of chloroplast membranes of higher plants? Frontiers in Plant Science. 2018;9:126.
73. Röös E, et al. Greedy or needy? Land use and climate impacts of food in 2050 under different livestock futures. Glob Environ Chang. 2017;47:1–12.
74. Ruelland E, Valentova O. Editorial: Lipid signaling in plant development and responses to environmental stresses. Front Plant Sci. 2016;7:324.
75. Sakaki T, et al. Lipids and fatty acids in guard-cell protoplasts from Vicia faba leaves. Phytochemistry. 1995;40(4):1065–70.
76. Savary S, et al. The global burden of pathogens and pests on major food crops. Nat Ecol Evol. 2019;3(3):430–9.
77. Schaller H. New aspects of sterol biosynthesis in growth and development of higher plants. Plant Physiol Biochem. 2004;42(6):465–76.
78. Shah J. Lipids, lipases, and lipid-modifying enzymes in plant disease resistance. Annu Rev Phytopathol. 2005;43:229–60.
79. Shannon P, et al. Cytoscape: a software environment for integrated models of biomolecular interaction networks. Genome Res. 2003;13(11):2498–504.
80. Siebers M, et al. Lipids in plant–microbe interactions. Biochimica et Biophysica Acta (BBA) - Molecular and Cell Biology of Lipids. 2016;1861(9, Part B):1379–95.
81. Spassieva SD, Markham JE, Hille J. The plant disease resistance gene Asc-1 prevents disruption of sphingolipid metabolism during AAL-toxin-induced programmed cell death. Plant J. 2002;32(4):561–72.
82. Strasser R. Biological significance of complex N-glycans in plants and their impact on plant physiology. Front Plant Sci. 2014;5: 363.
83. Subramoni S, Suárez-Moreno ZR, Venturi V. Lipases as pathogenicity factors of plant pathogens. In: Timmis KN, editor. Handbook of hydrocarbon and lipid microbiology. Berlin: Springer; 2010. p. 3269–77.
84. Sui Z, et al. Cloning and expression analysis of some genes involved in the phosphoinositide and phospholipid signaling pathways from maize (Zea mays L.). Gene. 2008;426(1–2):47–56.
85. Thomas R, et al. Soybean root suberin: anatomical distribution, chemical composition, and relationship to partial resistance to Phytophthora sojae. Plant Physiol. 2007;144(1):299–311.
86. Turner M, et al. Dissection of bacterial wilt on Medicago truncatula revealed two type III secretion system effectors acting on root infection process and disease development. Plant Physiol. 2009;150(4):1713–22.
87. Vailleau F, et al. Characterization of the interaction between the bacterial wilt pathogen Ralstonia solanacearum and the model legume plant Medicago truncatula. Molecular Plant-Microbe Interactions®. 2007;20(2):159–67.
88. Valitova JN, Sulkarnayeva AG, Minibayeva FV. Plant sterols: diversity, biosynthesis, and physiological functions. Biochem Mosc. 2016;81(8):819–34.
89. van Dam NM, Bouwmeester HJ. Metabolomics in the rhizosphere: tapping into belowground chemical communication. Trends Plant Sci. 2016;21(3):256–65.
90. van Meer G, Voelker DR, Feigenson GW. Membrane lipids: where they are and how they behave. Nat Rev Mol Cell Biol. 2008;9(2):112–24.
91. Velásquez AC, Castroverde CDM, He SY. Plant-pathogen warfare under changing climate conditions. Current biology : CB. 2018;28(10):R619–34.
92. Venegas-Molina J, et al. Induced tolerance to abiotic and biotic stresses of broccoli and Arabidopsis after treatment with elicitor molecules. Sci Rep. 2020;10(1):10319.
93. Wang T, Zabotina O, Hong M. Pectin-cellulose interactions in Arabidopsis primary cell wall from two-dimensional magic-angle-spinning solid-state NMR. Biochemistry. 2012;51:9846.
94. Wang K, et al. Phytosterols play a key role in plant innate immunity against bacterial pathogens by regulating nutrient efflux into the apoplast. Plant Physiol. 2012;158(4):1789–802.
95. Watt MJ, Steinberg GR. Regulation and function of triacylglycerol lipases in cellular metabolism. Biochemical Journal. 2008;414(3):313–25.
96. Wrather JA, Stienstra WC, Koenning SR. Soybean disease loss estimates for the United States from 1996 to 1998. Can J Plant Path. 2001;23(2):122–31.
97. Xing J, et al. Coordination of phospholipid-based signaling and membrane trafficking in plant immunity. Trends Plant Sci. 2021;26(4):407–20.
98. Xu C, Shanklin J. Triacylglycerol metabolism, function, and accumulation in plant vegetative tissues. Annu Rev Plant Biol. 2016;67(1):179–206.
99. Xue H, Lozano-Durán R, Macho AP. Insights into the root invasion by the plant pathogenic bacterium Ralstonia solanacearum. Plants. 2020;9(4):516.
100. Yuan S, et al. Diacylglycerol kinase and associated lipid mediators modulate rice root architecture. New Phytol. 2019;223(1):261–76.
101. Zhang Q, Xiao S. Lipids in salicylic acid-mediated defense in plants: focusing on the roles of phosphatidic acid and phosphatidylinositol 4-phosphate. Front Plant Sci. 2015;6:387–387.

Publisher's Note